

Solving Einstein's equation numerically on manifolds with arbitrary spatial topologies

Lee Lindblom, Béla Szilágyi, and Nicholas W. Taylor

Theoretical Astrophysics 350-17, California Institute of Technology, Pasadena, California 91125, USA

(Dated: February 27, 2022)

This paper develops a method for solving Einstein's equation numerically on multicube representations of manifolds with arbitrary spatial topologies. This method is designed to provide a set of flexible, easy to use computational procedures that make it possible to explore the never before studied properties of solutions to Einstein's equation on manifolds with arbitrary topological structures. A new covariant, first-order symmetric-hyperbolic representation of Einstein's equation is developed for this purpose, along with the needed boundary conditions at the interfaces between adjoining cubic regions. Numerical tests are presented that demonstrate the long-term numerical stability of this method for evolutions of a complicated, time-dependent solution of Einstein's equation coupled to a complex scalar field on a manifold with spatial topology S^3 . The accuracy of these numerical test solutions is evaluated by performing convergence studies and by comparing the full nonlinear numerical results to the analytical perturbation solutions, which are also derived here.

PACS numbers: 04.25.D- 04.20.Gz 02.40.Ma 98.80.Jk

I. INTRODUCTION

Solving partial differential equations on manifolds with arbitrary spatial topologies presents a number of challenges beyond those required to solve those equations on subsets of R^3 . In a previous paper, Lindblom and Szilágyi [1] showed how systems of elliptic and hyperbolic partial differential equations for collections of tensor fields can be solved numerically on manifolds with arbitrary spatial topologies by using multicube representations of those manifolds. We review some of the basic features of that multicube method in Sec. II. In particular, we discuss how the global differentiable structure (needed to define what it means globally to have smooth tensor fields) can be defined conveniently for multicube manifolds. We also review what boundary conditions are needed at the interfaces between cubic regions and how these conditions are enforced for first-order symmetric-hyperbolic evolution systems.

In Sec. III we develop a new (spatially) covariant, first-order symmetric-hyperbolic representation of the Einstein system that can be used on manifolds with arbitrary spatial topologies. The standard generalized-harmonic representation of Einstein's equation [2] is a special case of these new covariant representations on manifolds whose spatial slices are subsets of R^3 . Given this new representation of the Einstein system, it is straightforward to adapt the multicube methods developed by Lindblom and Szilágyi [1] to the Einstein case. In particular, the explicit boundary conditions that must be applied to the characteristic fields of this system at the interface boundaries between adjoining cubic regions are presented in Sec. III.

The long-term numerical stability of these methods is tested in Secs. IV–VI by studying solutions to Einstein's equation coupled to a complex Klein-Gordon scalar field. There exists a static solution to this system of equations whose spatial geometry is the standard round metric on

S^3 . This solution is therefore a (new) representation of the Einstein static universe. The Einstein static universe has a well-known physical instability that causes the universe to expand without bound or to collapse to a singularity on a fairly short time scale (cf. Ref. [3]). Our numerical tests of the coupled Einstein-Klein-Gordon system, described in Sec. IV, reproduce this well-known result.

One important goal of this paper is to study the long-term numerical stability of our implementation of the multicube methods. Since the Einstein-Klein-Gordon static universe solution is unstable, we introduce unphysical mode-damping forces into the Einstein and Klein-Gordon equations that are designed to exponentially suppress the two unstable modes of this solution. One of these unstable modes is the well-known spatially homogeneous physical instability of the Einstein static universe, while the other is a dipole instability that exists in the particular coordinate gauge used in our tests. These mode-damping forces, described in detail in Sec. V, leave untouched all of the rich dynamics of the Einstein-Klein-Gordon evolution equations, except for the degrees of freedom associated with the unstable modes. With the addition of these mode-damping forces, we are able to perform long-term evolutions (about 160 light-crossing times) of the Einstein static universe. The results of these tests, described in Sec. V, show that our implementation of the multicube method is stable and convergent, even on such very long time scales. We show that the constraints of this system, as well as the unphysical mode-damping forces, converge (exponentially quickly) toward zero as the spatial resolution of the numerical solutions is increased.

Finally, we test the accuracy and numerical stability of our implementation of the multicube method in Sec. VI by studying a complicated, time-dependent solution of the coupled Einstein-Klein-Gordon system. We derive the general solution to these equations analyti-

cally for first-order perturbations of the Einstein-Klein-Gordon static universe solution. These analytical solutions are then used to construct initial data composed of a superposition of 15 distinct modes. We evolve these initial data numerically and demonstrate stability and convergence. We show that the constraints of the system and the magnitudes of the unphysical mode-damping forces converge exponentially toward zero as the spatial resolution is increased. We measure the accuracy of the numerical solutions by comparing them with the analytical first-order perturbation solutions. We show that the differences between these two solutions converge toward zero, until these differences reach the level of the neglected quadratic terms in the analytical perturbation solution. These accuracy and stability tests are carried out for this complicated time-dependent solution for about 160 light-crossing times of the solution.

Solving Einstein's equation numerically on manifolds with arbitrary spatial topologies requires a number of computational tools beyond those needed to solve problems on manifolds having spatial slices which can be embedded in R^3 . In particular, smooth tensor fields must be represented in a way that does not depend on the existence of a single, smooth global coordinate system. To our knowledge, the methods developed by Lindblom and Szilágyi [1] and applied here to Einstein's equation are the first numerical methods to appear in the literature that are capable of solving these equations on arbitrary manifolds. As far as we know, Bentivegna and Korzynski [4–6] give the only other published results of fully three-dimensional numerical solutions of Einstein's equations on manifolds with nontrivial topologies. They evolve Einstein's equation in vacuum on manifolds having spatial topologies S^3 and T^3 , with black hole lattice solutions. They avoid the generic problem of solving equations on manifolds with arbitrary topologies by embedding each of their spatial manifolds¹ in R^3 and using its global Cartesian coordinates to represent smooth tensors. They then solve Einstein's equation numerically in R^3 using the standard tools of numerical relativity.

II. REVIEW OF THE MULTICUBE METHOD

The most useful manifolds for solving Einstein's equation numerically are those which admit globally hyperbolic causal structures. These manifolds have topologies of the form $R \times \Sigma$, where Σ is a three-dimensional manifold. The multicube method of representing three-dimensional manifolds with arbitrary topologies consists of three basic elements: (i) a collection of nonoverlapping cubic blocks \mathcal{B}_A that cover the manifold, (ii) a collection

of maps $\Psi_{B\beta}^{A\alpha}$ that specify how the faces of the blocks are connected together to create the desired topology, and (iii) a smooth positive-definite reference metric \hat{g}_{ij} used to determine the differentiable structure of the manifold. We devote most of the remainder of this section to a discussion of these basic elements of the multicube method. In addition, we give a brief review of the interface boundary conditions needed to solve first-order symmetric-hyperbolic evolution systems, like Einstein's equation, on multicube manifolds.

A. Multicube structures

An arbitrary (three-dimensional) manifold Σ can be subdivided into a collection of regions, each of which can be mapped smoothly into a cube \mathcal{B}_A in R^3 (cf. Ref. [1]). We use upper-case latin indices $\{A, B, \dots\}$ with $A = \{1, 2, \dots, N\}$ to label these regions and their images \mathcal{B}_A in R^3 . These regions overlap in Σ only along the boundaries between neighboring regions. It is convenient to choose the images of these regions \mathcal{B}_A to be cubes of uniform coordinate size, L , which are all oriented along the same global Cartesian coordinate axes in R^3 . In this case the cube \mathcal{B}_A can be specified simply by giving the location of its center $\vec{c}_A = (c^x_A, c^y_A, c^z_A)$ in R^3 . It is also convenient to arrange the cubes \mathcal{B}_A so they intersect (if at all) in R^3 only at points on faces where the corresponding regions touch in Σ .

This collection of cubes \mathcal{B}_A provides the basic framework on which a multicube representation of the manifold Σ can be constructed. Each point in the interior of one of the cubes represents a unique point in Σ . In addition, each point in Σ is the inverse image of at least one point in the closure of $\cup_A \mathcal{B}_A$. The Cartesian coordinates of R^3 therefore provide a global way of identifying points in Σ . We use the notation $x^i = \{x, y, z\}$ to denote these coordinates, where latin indices $\{i, j, k, l, \dots\}$ are used to denote spatial quantities.

B. Interface boundary maps

The topological structure of the manifold Σ determines how the cubic regions \mathcal{B}_A are connected together. Conversely, the topological structure of a multicube manifold is determined by giving a collection of maps $\Psi_{B\beta}^{A\alpha}$ that specify how the points on the faces of each cubic region are identified with those of its neighbors [1]. We use the notation $\Psi_{B\beta}^{A\alpha}$ to represent the map from the $\partial_\alpha \mathcal{B}_A$ face of cube \mathcal{B}_A to the $\partial_\beta \mathcal{B}_B$ face of cube \mathcal{B}_B . We use lower-case greek indices $\{\alpha, \beta, \dots\}$ with $\alpha = \{\pm x, \pm y, \pm z\}$ to label the faces of each cube. The cubes \mathcal{B}_A are chosen to be aligned with the global Cartesian coordinate axes in R^3 , so the region boundary faces are always located at constant spatial coordinate surfaces. For example, the boundary $\partial_\alpha \mathcal{B}_A$ is assumed to be a surface of constant coordinate $x^\sigma_A = x^\alpha_A$, where the index $\sigma = |\alpha|$ denotes

¹ One of the black hole interiors in the Bentivegna and Korzynski S^3 solution is excised, and a conformal transformation is applied to map its horizon to infinity in R^3 .

the fixed boundary-surface coordinate. This boundary surface is identified with the boundary $\partial_\beta \mathcal{B}_B$, a surface of constant coordinate $x_B^\sigma = x_B^{|\beta|}$, via the map $\Psi_{B\beta}^{A\alpha}$.

The map $\Psi_{B\beta}^{A\alpha}$ that takes the Cartesian coordinates x_B^j of points in $\partial_\beta \mathcal{B}_B$ to the Cartesian coordinates x_A^i of points in $\partial_\alpha \mathcal{B}_A$ can be chosen to have the form of a simple translation plus rotation and/or reflection (cf. Ref. [1]):

$$x_A^i = c_A^i + f_\alpha^i + C_{B\beta j}^{A\alpha i} (x_B^j - c_B^j - f_\beta^j). \quad (1)$$

The vector $c_A^i + f_\alpha^i$ is the location of the center of the face $\partial_\alpha \mathcal{B}_A$, and $C_{B\beta j}^{A\alpha i}$ is the combined spatial rotation and reflection matrix needed to match the face $\partial_\alpha \mathcal{B}_A$ to the face $\partial_\beta \mathcal{B}_B$ in the desired way. The vectors $c_A^i + f_\alpha^i$ and matrices $C_{B\beta j}^{A\alpha i}$ in these maps are constants determined once and for all by the topology of the particular manifold. These maps are smooth for the coordinates x^k within the boundary surface, i.e., for those with $k \neq \sigma$. For the normal surface coordinate x^σ , however, the maps are only continuous and not (in general) differentiable.

The multicube Cartesian coordinates x_A^i on the 3-manifold Σ can be extended naturally to coordinates on the spacetime $R \times \Sigma$: $x_A^a = \{t_A, x_A^i\}$, where latin indices from the beginning of the alphabet, $\{a, b, \dots\}$ with $a = \{t, x, y, z\}$, denote spacetime quantities. The maps $\Psi_{B\beta}^{A\alpha}$ defined above can be extended in a natural way to include the equation for the continuity of the time coordinate across region boundaries, $t_A = t_B$. The full spacetime coordinate transformation map can then be written in the compact, four-dimensional notation

$$x_A^a = c_A^a + f_\alpha^a + C_{B\beta b}^{A\alpha a} (x_B^b - c_B^b - f_\beta^b), \quad (2)$$

where $c_A^t + f_\alpha^t = 0$, $C_{B\beta b}^{A\alpha t} = \delta_b^t$, and $C_{B\beta t}^{A\alpha a} = \delta_t^a$.

Explicit expressions for the multicube representations of the 3-manifolds T^3 , $S^1 \times S^2$, and S^3 are described in detail in Ref. [1]. In particular, specific expressions are given there for the collections of cubic regions \mathcal{B}_A , the vectors c_A^i and f_α^i , and the interface boundary transformation matrices $C_{B\beta j}^{A\alpha i}$, needed to construct the multicube representation of each of these manifolds.

C. Reference metrics

Tensor fields can be represented on multicube manifolds by giving their components (expressed in the global coordinate basis of R^3) as functions of the global Cartesian coordinates. Within each coordinate region \mathcal{B}_A , the components of smooth tensor fields are smooth functions of these coordinates x_A^a . Additional structure must be provided, however, that determines how to transform continuous, differentiable, and smooth tensor fields across the interface boundaries between regions in multicube manifolds. One way to fix this differentiable structure is to specify a smooth, static spacetime metric, which we denote as $\tilde{\psi}_{ab}$ (cf. Ref. [1]). Like other smooth vector and tensor fields, the components of $\tilde{\psi}_{ab}$ might be

discontinuous across the boundaries of the cubic block regions when written in terms of the global multicube Cartesian coordinate basis. However, the components of $\tilde{\psi}_{ab}$ must be smooth functions in any smooth atlas of overlapping coordinate charts. The numerical examples studied in this paper solve Einstein's equation on a manifold with the topology of a three-sphere, $\Sigma = S^3$. For these examples, the multicube representation of the standard round-sphere metric on S^3 can be used to construct a reference metric (cf. Ref. [1]). Smooth multicube reference metrics are also given in Ref. [1] for manifolds with spatial topologies T^3 and $S^1 \times S^2$. In a future paper we will describe an algorithm for constructing smooth reference metrics $\tilde{\psi}_{ab}$ on any multicube manifold.

It is easy to construct covectors that are normal to the boundaries of the multicube regions: $\tilde{n}_{Aa} \propto \partial_a x_A^\sigma$. Given a smooth reference metric $\tilde{\psi}_{ab}$, these covectors can be normalized to be outward pointing and to have unit length: $\tilde{n}_A^a \tilde{n}_A^b \tilde{\psi}_{ab} = 1$ and $\tilde{n}_{Aa} = \tilde{\psi}_{ab} \tilde{n}_A^b$. Let \tilde{n}_A^a denote the outward-directed unit normal to the boundary $\partial_\alpha \mathcal{B}_A$, and \tilde{n}_B^a the outward-directed unit normal to $\partial_\beta \mathcal{B}_B$. Since the reference metric $\tilde{\psi}_{ab}$ is smooth, these normal vectors (up to sign) represent the same vector at the corresponding points on each side of identified boundaries. The transformation law that maps smooth tensor fields across interface boundaries must therefore be constructed to transform \tilde{n}_B^a into $-\tilde{n}_A^a$. In contrast, continuous vector fields u_A^a that are tangent to the boundary, i.e., $u_A^a \tilde{n}_A^b \tilde{\psi}_{ab} = 0$, should transform using the standard Jacobian of the map $\Psi_{B\beta}^{A\alpha}$ in Eq. (2): $u_A^a = C_{B\beta b}^{A\alpha a} u_B^b$. It is straightforward then to construct the transformations, effectively Jacobians, needed to transform arbitrary tensor fields from the region boundary $\partial_\beta \mathcal{B}_B$ to $\partial_\alpha \mathcal{B}_A$:

$$J_{B\beta b}^{A\alpha a} = C_{B\beta c}^{A\alpha a} (\delta_b^c - \tilde{n}_B^c \tilde{n}_{Bb}) - \tilde{n}_A^a \tilde{n}_{Bb}, \quad (3)$$

$$J_{A\alpha a}^{*B\beta b} = (\delta_a^c - \tilde{n}_{Aa} \tilde{n}_A^c) C_{A\alpha c}^{B\beta b} - \tilde{n}_{Aa} \tilde{n}_B^b. \quad (4)$$

These effective Jacobians transform the background surface normals correctly,

$$\tilde{n}_A^a = -J_{B\beta b}^{A\alpha a} \tilde{n}_B^b, \quad (5)$$

$$\tilde{n}_{Aa} = -J_{A\alpha a}^{*B\beta b} \tilde{n}_{Bb}, \quad (6)$$

and they also transform the components of vectors u^a that are tangent to the boundary correctly,

$$u_A^a = J_{B\beta b}^{A\alpha a} u_B^b = C_{B\beta b}^{A\alpha a} u_B^b, \quad (7)$$

using the rotation/reflection matrix $C_{B\beta b}^{A\alpha a}$ from the surface coordinate map. The Jacobian and its dual are also inverses of one another:

$$\delta_{Ab}^{Aa} = J_{B\beta c}^{A\alpha a} J_{A\alpha b}^{*B\beta c}. \quad (8)$$

We introduce the notation $\langle v_B^a \rangle_A$ and $\langle w_{Ba} \rangle_A$ to denote the result of transforming these vector and covector fields from the boundary of region B to the corresponding

points on the boundary of region A :

$$\langle v_B^a \rangle_A = J_{B\beta b}^{A\alpha a} v_B^b, \quad (9)$$

$$\langle w_{Ba} \rangle_A = J_{A\alpha a}^{*B\beta b} w_{Bb}. \quad (10)$$

The necessary and sufficient conditions for the continuity of these fields across interface boundaries are $v_A^a = \langle v_B^a \rangle_A$ and $w_{Aa} = \langle w_{Ba} \rangle_A$. The appropriate transformation laws for tensor fields are obtained by applying the effective Jacobian to each index of the tensor. For example, the physical spacetime metric ψ_{ab} , which will generally be different than the static reference metric $\tilde{\psi}_{ab}$, transforms across interface boundaries as follows:

$$\langle \psi_{Bab} \rangle_A = J_{A\alpha a}^{*B\beta c} J_{A\alpha b}^{*B\beta d} \psi_{Bcd}. \quad (11)$$

The continuity of the spacetime metric across this boundary is the statement that $\psi_{Aab} = \langle \psi_{Bab} \rangle_A$.

The rules for transforming the derivatives of tensors across interface boundaries can be determined by introducing the covariant derivative $\tilde{\nabla}_a$ that is compatible with the smooth reference metric, i.e., $\tilde{\nabla}_c \tilde{\psi}_{ab} = 0$. The covariant derivatives of smooth tensors are tensors, so these derivatives are transformed across region boundaries using the effective Jacobian $J_{B\beta b}^{A\alpha a}$ defined above. In particular, the transformations of the covariant derivatives of the vector v^a and covector w_a are given by the expressions

$$\begin{aligned} \langle \tilde{\nabla}_a v_B^b \rangle_A &= J_{A\alpha a}^{*B\beta c} J_{B\beta d}^{A\alpha b} \tilde{\nabla}_c v_B^d, \\ \langle \tilde{\nabla}_a w_{Bb} \rangle_A &= J_{A\alpha a}^{*B\beta c} J_{A\alpha b}^{*B\beta d} \tilde{\nabla}_c w_{Bd}. \end{aligned}$$

Tensor fields with continuous derivatives therefore satisfy the continuity conditions $\tilde{\nabla}_a v_A^b = \langle \tilde{\nabla}_a v_B^b \rangle_A$ and $\tilde{\nabla}_a w_{Ab} = \langle \tilde{\nabla}_a w_{Bb} \rangle_A$. These transformation laws can be generalized to tensor fields of arbitrary rank in the obvious way. In particular, the transformation of the derivatives of the spacetime metric is given by

$$\langle \tilde{\nabla}_c \psi_{Bab} \rangle_A = J_{A\alpha c}^{*B\beta d} J_{A\alpha a}^{*B\beta e} J_{A\alpha b}^{*B\beta f} \tilde{\nabla}_d \psi_{Bef}.$$

Smooth tensor fields are defined to be those having continuous derivatives of all orders.

D. Boundary conditions for hyperbolic systems

A first-order symmetric-hyperbolic system of equations for the dynamical fields u^A (assumed here to be a collection of tensor fields) can be written in the form

$$\partial_t u^A + A^{kA}{}_{\mathcal{B}}(\mathbf{x}, \mathbf{u}) \tilde{\nabla}_k u^{\mathcal{B}} = F^A(\mathbf{x}, \mathbf{u}), \quad (12)$$

where the characteristic matrix, $A^{kA}{}_{\mathcal{B}}(\mathbf{x}, \mathbf{u})$, and the source term, $F^A(\mathbf{x}, \mathbf{u})$, may depend on the spacetime coordinates x^a and the fields u^A , but not their derivatives. The script indexes $\{A, B, C, \dots\}$ in these expressions label the components of the collection of tensor fields that make up u^A . These systems are called symmetric

because, by assumption, there exists a positive-definite metric on the space of fields, $S_{\mathcal{A}\mathcal{B}}$, that can be used to transform the characteristic matrix into a symmetric form: $S_{\mathcal{A}C} A^{kC}{}_{\mathcal{B}} \equiv A_{\mathcal{A}\mathcal{B}}^k = A_{\mathcal{B}\mathcal{A}}^k$.

Boundary conditions for symmetric-hyperbolic systems must be imposed on the incoming characteristic fields of the system. The characteristic fields $\hat{u}^{\mathcal{K}}$ (whose index \mathcal{K} labels the collection of characteristic fields) are projections of the dynamical fields u^A onto the matrix of left eigenvectors of the characteristic matrix (cf. Refs. [2, 7]):

$$\hat{u}^{\mathcal{K}} = e^{\mathcal{K}}{}_{\mathcal{A}}(\mathbf{n}) u^A. \quad (13)$$

The matrix of eigenvectors $e^{\mathcal{K}}{}_{\mathcal{A}}(\mathbf{n})$ is defined by the equation

$$e^{\mathcal{K}}{}_{\mathcal{A}}(\mathbf{n}) n_k A^{kA}{}_{\mathcal{B}}(u) = v_{(\mathcal{K})} e^{\mathcal{K}}{}_{\mathcal{B}}(\mathbf{n}), \quad (14)$$

where the covector n_k that appears in this definition is the outward-pointing unit normal to the surface on which the characteristic fields are evaluated. The eigenvalues $v_{(\mathcal{K})}$ are often referred to as the characteristic speeds of the system. The characteristic fields $\hat{u}^{\mathcal{K}}$ represent the independent dynamical degrees of freedom at the boundaries. These characteristic fields propagate at the speeds $v_{(\mathcal{K})}$ (in the short wavelength limit), so boundary conditions must be given for each incoming characteristic field, i.e., for each field with speed $v_{(\mathcal{K})} < 0$. No boundary condition is required (or allowed) for outgoing characteristic fields, i.e., any field with $v_{(\mathcal{K})} \geq 0$.

The boundary conditions on the dynamical fields u^A that ensure the equations are satisfied across the faces of adjoining cubic regions are quite simple: data for the incoming characteristic fields at the boundary of one region are supplied by the outgoing characteristic fields from the neighboring region. The boundary conditions at an interface between cubic regions require that the dynamical fields u_A^A in region \mathcal{B}_A be transformed into the representation used in the neighboring region \mathcal{B}_B . When the dynamical fields u^A are a collection of tensor fields (as assumed here), their components are transformed from one coordinate representation to another using the Jacobians of the transformation as described in Eqs. (9) and (10). In this case, the needed boundary conditions can be stated precisely for hyperbolic evolution problems: Consider two cubic regions \mathcal{B}_A and \mathcal{B}_B whose boundaries $\partial_\alpha \mathcal{B}_A$ and $\partial_\beta \mathcal{B}_B$ are identified by the map $\Psi_{\beta B}^{\alpha A}$ as defined in Eq. (2). The required boundary conditions on the dynamical fields u_A^A consist of fixing the incoming characteristic fields $\hat{u}_A^{\mathcal{K}}$ (i.e., those with speeds $v_{(\mathcal{K})} < 0$) at the boundary $\partial_\alpha \mathcal{B}_A$ with data, $u_B^{\mathcal{B}}$, from the fields on the neighboring boundary $\partial_\beta \mathcal{B}_B$:

$$\hat{u}_A^{\mathcal{K}} = \langle e^{\mathcal{K}}{}_{\mathcal{A}}(\mathbf{n}) \rangle_A \langle u_B^A \rangle_A. \quad (15)$$

The matrix of eigenvectors, $\langle e^{\mathcal{K}}{}_{\mathcal{A}}(\mathbf{n}) \rangle_A$, that appears in Eq. (15) is to be constructed with the fields from region \mathcal{B}_B that have been transformed into region \mathcal{B}_A where

the boundary condition is to be imposed. This boundary condition must be applied to each incoming characteristic field on each internal cube face—i.e., on each face that is identified with the face of a neighboring region.

III. COVARIANT FIRST-ORDER EINSTEIN EVOLUTION SYSTEM

Einstein's equation determines the spacetime metric ψ_{ab} by equating the Einstein curvature tensor to the stress-energy tensor of the matter in the spacetime. This equation is, of course, covariant. The standard first-order hyperbolic representations of Einstein's equation (e.g., Ref. [2]), however, are not covariant, because the auxiliary dynamical fields introduced to make the system first order are not tensors. This lack of covariance has not caused any problems (that we know of) in the codes that solve these noncovariant equations on spatial manifolds that can be embedded in R^3 , e.g., for binary black-hole spacetimes. However, our attempts to use these noncovariant representations for numerical evolutions on manifolds with nontrivial spatial topologies failed. We were unable to achieve stable and convergent evolutions, at the interface boundaries in particular. These problems disappeared when we adopted the spatially covariant representation of the first-order Einstein evolution system described in the remainder of this section. The interface boundary conditions needed for this new covariant representation are precisely those described in Sec. IID for any hyperbolic system whose dynamical fields are tensors.

Let ψ_{ab} denote the physical spacetime metric that is determined by solving Einstein's equation, and let Γ_{bc}^a and ∇_a denote the connection and covariant derivative associated with ψ_{ab} . Let $\tilde{\psi}_{ab}$ denote a smooth static reference metric, and let $\tilde{\Gamma}_{bc}^a$ and $\tilde{\nabla}_a$ denote the connection and covariant derivative associated with $\tilde{\psi}_{ab}$. It is straightforward to show that the physical Ricci curvature R_{ab} associated with ψ_{ab} satisfies the identity

$$R_{ab} = -\frac{1}{2}\psi^{cd}\tilde{\nabla}_c\tilde{\nabla}_d\psi_{ab} + \nabla_{(a}\Delta_{b)} - \psi^{cd}\tilde{R}^e{}_{cd(a}\psi_{b)e} + \psi^{cd}\psi^{ef}\left(\tilde{\nabla}_e\psi_{ca}\tilde{\nabla}_f\psi_{bd} - \Delta_{ace}\Delta_{bdf}\right), \quad (16)$$

where Δ_{abc} is the tensor that describes the difference between the connections:

$$\begin{aligned} \Delta_{abc} &= \psi_{ad}\left(\Gamma_{bc}^d - \tilde{\Gamma}_{bc}^d\right) \\ &= \frac{1}{2}\left(\tilde{\nabla}_b\psi_{ac} + \tilde{\nabla}_c\psi_{ab} - \tilde{\nabla}_a\psi_{bc}\right). \end{aligned} \quad (17)$$

The vector Δ_a is defined as $\Delta_a = \psi^{bc}\Delta_{abc}$, and $\tilde{R}^d{}_{abc}$ is the reference Riemann curvature associated with $\tilde{\psi}_{ab}$. Note that Eq. (16) reduces to Eq. (4) of Ref. [2] for the case where the reference metric is the flat Minkowski metric $\tilde{\psi}_{ab} = \eta_{ab}$ expressed in Cartesian coordinates.

In analogy with the generalized harmonic representations of Einstein's equation (e.g., Ref. [2]), the gauge (or

coordinate) conditions are fixed in this covariant evolution system by setting Δ_a to be a fixed gauge source function:

$$\Delta_a = -H_a. \quad (18)$$

We assume that this gauge source function $H_a = H_a(\psi, \tilde{\psi}, \partial^k\tilde{\psi}, x)$ may depend on the physical metric ψ_{ab} (but not its derivatives) and the reference metric $\tilde{\psi}_{ab}$ (including its derivatives if desired), as well as the spacetime coordinates x^a . This gauge condition becomes a constraint of the system:

$$\mathcal{C}_a = \Delta_a + H_a. \quad (19)$$

The covariant vacuum evolution equation therefore satisfies the standard generalized harmonic evolution equation:

$$0 = R_{ab} - \nabla_{(a}\mathcal{C}_{b)}. \quad (20)$$

The standard argument (cf. Ref. [2]) using the Bianchi identities implies that the constraint \mathcal{C}_a satisfies the evolution equation

$$0 = \nabla^b\nabla_b\mathcal{C}_a + \mathcal{C}^b\nabla_{(a}\mathcal{C}_{b)}, \quad (21)$$

which is also identical to the standard generalized harmonic case. It follows that the Pretorius-Gundlach [8–10] constraint-damping mechanism can be applied to the covariant evolution system without modification. In particular, we add the constraint-damping terms:

$$0 = R_{ab} - \nabla_{(a}\mathcal{C}_{b)} + \gamma_0\left[t_{(a}\mathcal{C}_{b)} - \frac{1}{2}\psi_{ab}t^c\mathcal{C}_c\right], \quad (22)$$

where t^a is a timelike vector field, and γ_0 is a constant. The constraint evolution implied by the covariant evolution system with constraint damping, Eq. (22), is obtained by using the Bianchi identities. The result is the evolution system

$$0 = \nabla^b\nabla_b\mathcal{C}_a - 2\gamma_0\nabla^b\left[t_{(b}\mathcal{C}_{a)}\right] + \mathcal{C}^b\nabla_{(a}\mathcal{C}_{b)} - \frac{1}{2}\gamma_0t_a\mathcal{C}^b\mathcal{C}_b, \quad (23)$$

which is a damped wave equation for small, short-wavelength \mathcal{C}_a when $\gamma_0 > 0$. The covariant vacuum Einstein equation, including the constraint-damping terms, reduces therefore to the following manifestly hyperbolic system:

$$\begin{aligned} \psi^{cd}\tilde{\nabla}_c\tilde{\nabla}_d\psi_{ab} &= -2\nabla_{(a}H_{b)} - 2\psi^{cd}\tilde{R}^e{}_{cd(a}\psi_{b)e} \\ &\quad + 2\psi^{cd}\psi^{ef}\left(\tilde{\nabla}_e\psi_{ca}\tilde{\nabla}_f\psi_{bd} - \Delta_{ace}\Delta_{bdf}\right) \\ &\quad + \gamma_0\left[2\delta_{(a}^c t_{b)} - \psi_{ab}t^c\right](H_c + \Delta_c). \end{aligned} \quad (24)$$

This equation (minus the constraint-damping terms) was derived previously by Ruiz, Rinne and Sarbach [11], who used it in their analysis of boundary conditions, and by Brown [12], who used it to derive an action principle for

this second-order covariant generalized harmonic formulation of Einstein's equation.

The idea now is to transform Eq. (24) into a spatially covariant symmetric-hyperbolic first-order evolution system. To that end, we introduce the physical timelike normal, t^a , which satisfies $\psi_{ab}t^at^b = -1$, and which can be expressed in terms of the lapse N and shift N^k of the physical metric: $t^a\partial_a = N^{-1}(\partial_t - N^k\partial_k)$. We then define the first-order variables, Π_{ab} and Φ_{iab} :

$$\Pi_{ab} = -t^c\tilde{\nabla}_c\psi_{ab}, \quad (25)$$

$$\Phi_{iab} = \tilde{\nabla}_i\psi_{ab}, \quad (26)$$

where the indices $\{i,j,k,\dots\}$ range only over the spatial coordinates, while the indices $\{a,b,c,d,\dots\}$ range over both space and time coordinates. The introduction of Φ_{iab} also implies the existence of a new constraint for the system:

$$\mathcal{C}_{iab} = \tilde{\nabla}_i\psi_{ab} - \Phi_{iab}. \quad (27)$$

We note that the constraint, \mathcal{C}_{iab} , like the first-order evolution fields, Π_{ab} and Φ_{iab} , is a tensor with respect to purely spatial coordinate transformations.

The spatially covariant first-order evolution equation for ψ_{ab} follows directly from the definition of Π_{ab} in Eq. (25):

$$\begin{aligned} \partial_t\psi_{ab} - (1 + \gamma_1)N^k\partial_k\psi_{ab} \\ = -N\Pi_{ab} - \gamma_1N^k\Phi_{kab} - 2(1 + \gamma_1)N^k\tilde{\Gamma}_{k(a}\tilde{\psi}_{b)j}. \end{aligned} \quad (28)$$

The constraint term $\gamma_1N^k\mathcal{C}_{kab}/N$, where γ_1 is an arbitrary constant, has been added to the definition of Π_{ab} to obtain Eq. (28). The particular choice $\gamma_1 = -1$ makes the system linearly degenerate, which implies that shocks will not form from smooth initial data [13]. Here the quantity $\tilde{\Gamma}_{bc}^a$ is the connection associated with the reference metric $\tilde{\psi}_{ab}$. We assume that this reference metric is static, $\partial_t\psi_{ab} = 0$, and that $\tilde{\psi}_{tt} = -1$ and $\tilde{\psi}_{ti} = 0$. It follows that all of the time components of $\tilde{\Gamma}_{bc}^a$ vanish, $\tilde{\Gamma}_{bc}^t = \tilde{\Gamma}_{tc}^a = 0$, in this case.

The spatially covariant first-order evolution equation for Π_{ab} follows from the second-order covariant evolution equation, Eq. (24):

$$\begin{aligned} \partial_t\Pi_{ab} - N^k\partial_k\Pi_{ab} + Ng^{ki}\partial_k\Phi_{iab} - \gamma_1\gamma_2N^k\partial_k\psi_{ab} \\ = 2N\psi^{cd}(g^{ij}\Phi_{ica}\Phi_{jdb} - \Pi_{ca}\Pi_{db} - \psi^{ef}\Delta_{ace}\Delta_{bdf}) \\ - 2N\nabla_{(a}H_{b)} - \frac{1}{2}Nt^ct^d\Pi_{cd}\Pi_{ab} - Nt^c\Pi_{ci}g^{ij}\Phi_{jab} \\ + N\gamma_0\left[2\delta_c^a t_b - \psi_{ab}t^c\right](H_c + \Delta_c) - \gamma_1\gamma_2N^i\Phi_{iab} \\ - 2N\psi^{ij}\tilde{R}^k{}_{ij(a}\tilde{\psi}_{b)k} - 2N^i\tilde{\Gamma}_{i(a}\tilde{\psi}_{b)j} + Ng^{ij}\tilde{\Gamma}_{ij}^k\Phi_{kab} \\ + 2Ng^{ij}\Phi_{ik(a}\tilde{\Gamma}_{b)j}^k - 2\gamma_1\gamma_2N^i\tilde{\Gamma}_{i(a}\tilde{\psi}_{b)j} \\ - 8\pi N(2T_{ab} - \psi_{ab}\psi^{cd}T_{cd}) - 2N\Lambda\psi_{ab}. \end{aligned} \quad (29)$$

In this expression, T_{ab} represents the stress-energy tensor of any matter that may be present in the solution, and

Λ is the cosmological constant. We use the notation g_{ab} for the spatial metric, $g_{ab} = \psi_{ab} + t_at_b$, which satisfies $g_{ab}t^b = 0$. The quantity g^{ij} is the inverse of the spatial metric $g_{ij} = \psi_{ij}$. The quantities Δ_{abc} and $\Delta_a = \psi^{bc}\Delta_{abc}$ that appear on the right side of Eq. (29) are to be written as functions of the first-order fields Π_{ab} and Φ_{iab} : i.e., the derivatives $\tilde{\nabla}_a\psi_{bc}$ that appear in the definition of Δ_{abc} , Eq. (17), are to be replaced by the expressions

$$\tilde{\nabla}_t\psi_{ab} = -N\Pi_{ab} + N^i\Phi_{iab}, \quad (30)$$

$$\tilde{\nabla}_i\psi_{ab} = \Phi_{iab}. \quad (31)$$

The derivation of the evolution equation for Π_{ab} , Eq. (29), also uses the identity $t^b\tilde{\nabla}_bt^a = \frac{1}{2}t^c(2\psi^{ab} + t^at^b)\Pi_{bc}$.

The spatially covariant first-order evolution equation for Φ_{iab} is obtained by requiring that the constraint \mathcal{C}_{iab} satisfy a damped, advection-type evolution equation:

$$t^c\tilde{\nabla}_c\mathcal{C}_{iab} = -\gamma_2\mathcal{C}_{iab}. \quad (32)$$

Choosing the constant $\gamma_2 > 0$ ensures that the constraint \mathcal{C}_{iab} is driven toward zero as the system evolves. This constraint-damping equation implies the following first-order evolution equation for Φ_{iab} :

$$\begin{aligned} \partial_t\Phi_{iab} - N^k\partial_k\Phi_{iab} + N\partial_i\Pi_{ab} - N\gamma_2\partial_i\psi_{ab} \\ = \frac{1}{2}Nt^ct^d\Phi_{icd}\Pi_{ab} + Ng^{jk}t^c\Phi_{ijc}\Phi_{kab} - N\gamma_2\Phi_{iab} \\ - N^j\tilde{\Gamma}_{ij}^k\Phi_{kab} - 2N^j\Phi_{ik(a}\tilde{\Gamma}_{b)j}^k + 2N\tilde{\Gamma}_{i(a}\tilde{\psi}_{b)j} \\ - 2N\gamma_2\tilde{\Gamma}_{i(a}\tilde{\psi}_{b)j} - 2N^k\psi_{j(a}\tilde{R}^j{}_{b)ik}. \end{aligned} \quad (33)$$

The derivation of this evolution equation uses the identity $\tilde{\nabla}_it^a = -\frac{1}{2}t^c(2\psi^{ab} + t^at^b)\Phi_{ibc}$.

The principal parts of a first-order evolution system are defined to be the terms that involve the derivatives of the fields. We use the notation $\partial_t u^A + A^{kA}{}_{\mathcal{B}}(\mathbf{x}, \mathbf{u})\tilde{\nabla}_k u^{\mathcal{B}} \simeq 0$ to denote the principal parts of the general first-order hyperbolic system described in Eq. (12). The principal parts of the spatially covariant first-order evolution system defined in Eqs. (28), (29), and (33) are therefore given by

$$\begin{aligned} \partial_t\psi_{ab} - (1 + \gamma_1)N^k\tilde{\nabla}_k\psi_{ab} &\simeq 0, \\ \partial_t\Pi_{ab} - N^k\tilde{\nabla}_k\Pi_{ab} + Ng^{ki}\tilde{\nabla}_k\Phi_{iab} - \gamma_1\gamma_2N^k\tilde{\nabla}_k\psi_{ab} &\simeq 0, \\ \partial_t\Phi_{iab} - N^k\tilde{\nabla}_k\Phi_{iab} + N\tilde{\nabla}_i\Pi_{ab} - N\gamma_2\tilde{\nabla}_i\psi_{ab} &\simeq 0. \end{aligned}$$

These terms are identical to the principal parts of the standard first-order generalized harmonic evolution system described in Ref. [2]. It follows that this spatially covariant first-order evolution system is symmetric hyperbolic with the standard symmetrizer [2]:

$$\begin{aligned} S_{\alpha\beta}du^\alpha du^\beta = m^{ab}m^{cd}(L^{-2}d\psi_{ac}d\psi_{bd} + d\Pi_{ac}d\Pi_{bd} \\ - 2\gamma_2d\psi_{ac}d\Pi_{bd} + g^{ij}d\Phi_{iac}d\Phi_{jbd}), \end{aligned} \quad (34)$$

where m^{ab} is any positive-definite metric (e.g., $m^{ab} = g^{ab} + t^at^b$, or even $m^{ab} = \delta^{ab}$) and L is a constant with

the dimension of a length. It follows that the characteristic fields and speeds of the spatially covariant first-order evolution system are identical to those of the noncovariant generalized harmonic system. In particular, the characteristic fields $\hat{u}^{\mathcal{K}} = \{\hat{u}_{ab}^0, \hat{u}_{ab}^{1\pm}, \hat{u}_{iab}^2\}$ are given by

$$\hat{u}_{ab}^0 = \psi_{ab}, \quad (35)$$

$$\hat{u}_{ab}^{1\pm} = \Pi_{ab} \pm n^i \Phi_{iab} - \gamma_2 \psi_{ab}, \quad (36)$$

$$\hat{u}_{iab}^2 = P_i^k \Phi_{kab}, \quad (37)$$

where $P_i^k = \delta_i^k - n_i n^k$. All of these characteristic fields are tensors with respect to spatial coordinate transformations. The characteristic fields \hat{u}_{ab}^0 have coordinate characteristic speed $-(1+\gamma_1)n_k N^k$, the fields $\hat{u}_{ab}^{1\pm}$ have speeds $-n_k N^k \pm N$, and the fields \hat{u}_{iab}^2 have speed $-n_k N^k$.

The first-order dynamical fields Π_{ab} and Φ_{iab} of the spatially covariant first-order evolution system are different from those used in the noncovariant generalized-harmonic evolution equations. These differences require that additional terms proportional to the reference connection $\tilde{\Gamma}_{bc}^a$ and its curvature \tilde{R}_{bcd}^a be added to the right sides of Eqs. (28), (29), and (33). But these additional terms do not affect the principal parts of the equations, the expressions for the characteristic fields in terms of the dynamical fields, or the characteristic speeds of the system. We also note that the reference metric can be chosen to be the Minkowski metric, $\psi_{ab} = \eta_{ab}$, on manifolds that admit a global flat metric (e.g., manifolds whose spatial slices are subsets of R^3). When expressed in terms of the global Cartesian coordinates that are available in such a case, the reference connection $\tilde{\Gamma}_{bc}^a$ and the reference curvature \tilde{R}_{bcd}^a both vanish identically. The spatially covariant first-order evolution system is then precisely the same as the standard noncovariant generalized harmonic system. The standard first-order generalized harmonic system is therefore a special case of the new covariant first-order system on manifolds that admit a flat reference metric.

The constraints \mathcal{C}_a and \mathcal{C}_{iab} defined in Eqs. (19) and (27) evolve according to Eqs. (21) and (32). As in the noncovariant generalized harmonic evolution system [2], the second-order evolution system for these constraints can be converted into a symmetric-hyperbolic first-order system by adding the following secondary constraints:

$$\mathcal{F}_a = t^c \nabla_c \mathcal{C}_a, \quad (38)$$

$$\mathcal{C}_{ia} = \nabla_i \mathcal{C}_a, \quad (39)$$

$$\mathcal{C}_{ijab} = 2\tilde{\nabla}_{[i} \mathcal{C}_{j]ab}. \quad (40)$$

Expressions for all the constraints \mathcal{C}_a , \mathcal{C}_{iab} , \mathcal{F}_a , \mathcal{C}_{ia} , and \mathcal{C}_{ijab} are given in Appendix A in terms of the dynamical fields of the system $u^A = \{\psi_{ab}, \Pi_{ab}, \Phi_{iab}\}$ and their spatial derivatives.

IV. EINSTEIN-KLEIN-GORDON STATIC UNIVERSE

The remainder of this paper is devoted to performing a number of simple numerical tests on the multicube methods described in Sec. II, using the spatially covariant representation of the Einstein system developed in Sec. III. Our primary goal here is to verify that our implementation of these methods in the SpEC code (developed by the SXS Collaboration, originally at Caltech and Cornell [14–17]) is numerically stable and convergent for long-time-scale evolutions. Most known solutions to Einstein’s equation on manifolds with compact spatial topologies collapse to a singularity or expand exponentially without bound on very short time scales. Neither of these types of solutions is well suited for testing the long-term stability of a numerical code. We have therefore focused our attention on one of the few known time-independent solutions on a manifold with compact spatial topology: the Einstein static universe.

The Einstein static universe is a time-independent (static) and spatially homogeneous solution to Einstein’s equation on the manifold $R \times S^3$:

$$\begin{aligned} ds^2 &= \psi_{ab}^0 dx^a dx^b \\ &\equiv -dt^2 + R_3^2 [d\chi^2 + \sin^2 \chi (d\theta^2 + \sin^2 \theta d\varphi^2)]. \end{aligned} \quad (41)$$

The spatial part of this geometry is just the standard round metric on S^3 . This metric satisfies Einstein’s gravitational field equation with source

$$R_{ab} - \frac{1}{2}\psi_{ab}R + \Lambda\psi_{ab} = 8\pi T_{ab}, \quad (42)$$

where Λ is the cosmological constant and T_{ab} is the stress-energy tensor of the matter present in the spacetime. The cosmological constant has the value $\Lambda = 1/R_3^2$ for the Einstein static universe, while the stress-energy tensor $T_{ab} = \rho \partial_a t \partial_b t$ corresponds to a pressureless “dust” with $\rho = 1/4\pi R_3^2$. Dynamical evolutions of spacetimes containing dust typically develop shell-crossing singularities [18]. Hence, dust is not particularly well suited for numerical tests using spectral methods, which require smooth solutions to achieve exponential convergence [19].

An alternate interpretation of the Einstein static universe can be constructed in which the matter part of the solution is generated by a complex Klein-Gordon scalar field instead of dust. The stress-energy tensor of a complex scalar field ϕ is given by

$$\begin{aligned} T_{ab} &= \frac{1}{2} (\nabla_a \phi \nabla_b \phi^* + \nabla_a \phi^* \nabla_b \phi) \\ &\quad - \frac{1}{2} \psi_{ab} (\psi^{cd} \nabla_c \phi \nabla_d \phi^* + \mu^2 \phi \phi^*), \end{aligned} \quad (43)$$

where ϕ^* is the complex conjugate of the field, and μ is its mass. This field satisfies the covariant Klein-Gordon equation,

$$\nabla^a \nabla_a \phi = \mu^2 \phi, \quad (44)$$

as a consequence of the stress-energy conservation law $\nabla^a T_{ab} = 0$. One solution to this scalar field equation in

the Einstein static universe is

$$\phi = \phi_0 e^{i\mu t}, \quad (45)$$

where ϕ_0 is a (complex) constant. This particular solution has a stress-energy tensor that can be used as the source term needed for an Einstein-Klein-Gordon static universe by taking $\Lambda = 1/R_3^2$ and $\mu^2|\phi_0|^2 = 1/4\pi R_3^2$. Note that only the product $|\phi_0|\mu$ is fixed, not their individual values. For our numerical tests, we use $\mu = 2/R_3$ so that $|\phi_0| = 1/\sqrt{16\pi}$. Also note that although the geometry of the Einstein-Klein-Gordon universe is static, the scalar field ϕ oscillates with frequency μ . In our numerical test evolutions, we use the value $R_3 = 1$ for the scale of the S^3 geometry.

The first test of our implementation of the multicube methods described in Sec. II is to evolve initial data for the coupled Einstein and Klein-Gordon evolution equations based on the static Einstein-Klein-Gordon universe solution. The spacetime manifold for this solution has the topology $R \times S^3$, so we use the round metric ψ_{ab}^0 of Eq. (41) as our smooth reference metric: $\tilde{\psi}_{ab} = \psi_{ab}^0$. The initial data for the dynamical fields of the Einstein evolution system, $u^\alpha = \{\psi_{ab}, \Pi_{ab}, \Phi_{iab}\}$, are constructed from the metric of the Einstein static universe solution. In particular, we take $\psi_{ab} = \psi_{ab}^0$ and $\Pi_{ab} = \Phi_{iab} = 0$ initially. The dynamical fields of the complex first-order Klein-Gordon system consist of the fields $u_\phi^\alpha = \{\phi, \Pi^\phi, \Phi_i^\phi\}$. The initial values of these fields for the Einstein-Klein-Gordon static universe solution are given by $\phi = \phi_0$, $\Pi^\phi = -i\mu\phi_0$, and $\Phi_i^\phi = 0$. We carry out the numerical evolutions of these fields using the multicube representation of S^3 developed in Ref. [1], which gives the explicit multicube expressions for the metric ψ_{ab}^0 , as well as the standard three-sphere angular coordinates χ , θ , and φ , in terms of the global multicube Cartesian coordinates.

Evolutions of Einstein's equation require appropriate gauge (i.e., coordinate) conditions to be specified. The gauge is specified in the spatially covariant first-order representation of the Einstein equation, described in Sec. III, using the gauge source covector H_a . The gauge condition is imposed with the covariant generalized harmonic condition: $H_a = -\Delta_{abc}\psi^{bc}$. It is straightforward to show that the static Einstein-Klein-Gordon solution satisfies this condition with $H_a = 0$. The gauge choices used in our numerical tests are harmonic gauge for the time coordinate and damped harmonic gauge [20] for the spatial coordinates:

$$H_t = 0, \quad (46)$$

$$H_i = -\mu_G N_i / N, \quad (47)$$

where μ_G is a constant that serves as the harmonic gauge damping parameter, N is the lapse, and N_i is the shift of the spacetime metric. This choice of gauge source function H_a depends only on the spacetime metric (and not its derivatives), so the covariant first-order representation of Einstein's equation is hyperbolic in this case. Note that this choice of gauge reduces to harmonic gauge

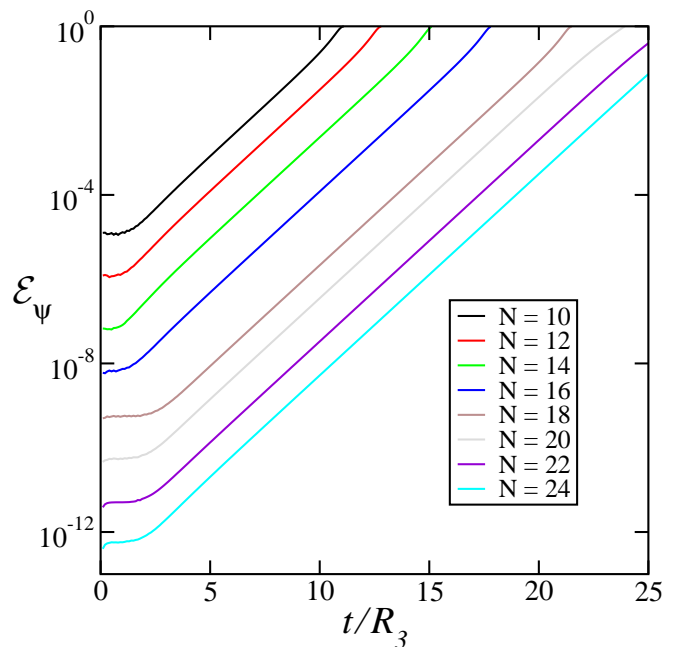


FIG. 1: Errors in the numerical evolution of the metric ψ_{ab} using initial data for the Einstein-Klein-Gordon static solution. Numerical resolution used in each spatial dimension of each cubic region is denoted by N .

$H_a = 0$ for the Einstein-Klein-Gordon static universe solution where $N = 1$ and $N_i = 0$.

The results of this first numerical test are illustrated in Figs. 1–3. Figure 1 shows the error in the metric \mathcal{E}_ψ as a function of time for evolutions using different spatial resolutions. The constant N , which appears in the labels of these figures, is the number of spectral basis functions used in the solution for each dimension of each cubic region \mathcal{B}_A . The error measure \mathcal{E}_ψ is defined by

$$\mathcal{E}_\psi^2 \equiv \frac{\int m^{ab} m^{cd} \Delta\psi_{ac} \Delta\psi_{bd} \sqrt{g} d^3x}{\int m^{ab} m^{cd} \psi_{ac}^N \psi_{bd}^N \sqrt{g} d^3x}, \quad (48)$$

where $\Delta\psi_{ab} = \psi_{ac}^N - \psi_{ac}^A$, ψ_{ab}^A , and ψ_{ab}^N represent the analytically and numerically determined metrics, and m^{ab} is a positive definite tensor, taken here to be $m^{ab} = \delta^{ab}$ in the global multicube Cartesian coordinates. This quantity measures the fractional accuracy of the numerically determined metric. Similarly, Fig. 2 shows the scalar field error measure, \mathcal{E}_ϕ , defined by

$$\mathcal{E}_\phi^2 \equiv \frac{\int |\Delta\phi|^2 \sqrt{g} d^3x}{\int |\phi^N|^2 \sqrt{g} d^3x}, \quad (49)$$

where $\Delta\phi = \phi^N - \phi^A$, and vertical bars denote the complex absolute value. Figure 3 shows the constraint errors of the combined Einstein and Klein-Gordon evolution equations. We combine these constraint errors into the single quantity \mathcal{C} , defined by

$$\mathcal{C}^2 \equiv \frac{\int \mathcal{C}_\psi^2 \sqrt{g} d^3x}{\int \mathcal{N}_\psi^2 \sqrt{g} d^3x} + \frac{\int \mathcal{C}_\phi^2 \sqrt{g} d^3x}{\int \mathcal{N}_\phi^2 \sqrt{g} d^3x}. \quad (50)$$

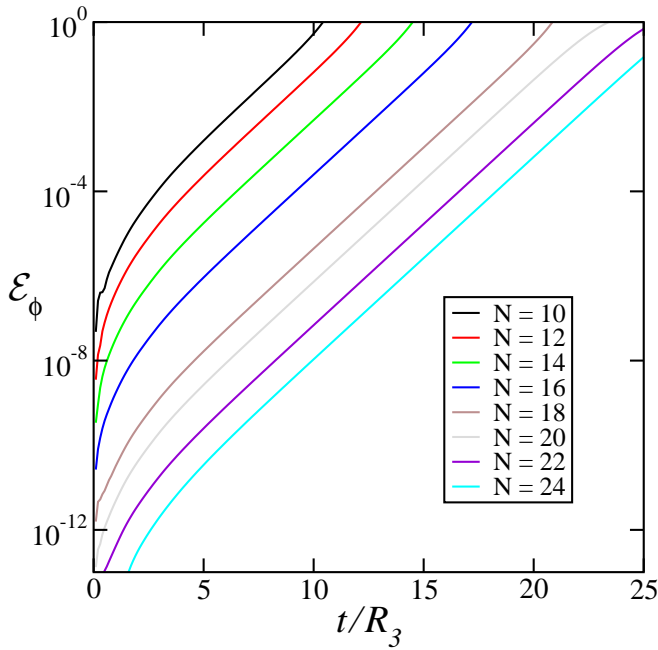


FIG. 2: Errors in the numerical evolution of the complex Klein-Gordon scalar field ϕ using initial data for the Einstein-Klein-Gordon static solution. Numerical resolution used in each spatial dimension of each cubic region is denoted by N .

The quantity \mathcal{C}_ψ measures the size of the constraint violations of the Einstein system, and \mathcal{N}_ψ measures the sizes of the spatial derivatives of the dynamical fields:

$$\mathcal{C}_\psi^2 \equiv m^{ab} \left(\mathcal{C}_a \mathcal{C}_b + \mathcal{F}_a \mathcal{F}_b + \tilde{g}^{ij} m^{cd} [\mathcal{C}_{iac} \mathcal{C}_{jbd} + \frac{1}{4} \tilde{g}^{kl} \mathcal{C}_{ikac} \mathcal{C}_{jlbcd}] \right), \quad (51)$$

$$\mathcal{N}_\psi^2 \equiv m^{ab} m^{cd} \tilde{g}^{ij} \left(\partial_i \psi_{ac} \partial_j \psi_{bd} + \partial_i \Pi_{ac} \partial_j \Pi_{bd} + \tilde{g}^{kl} \partial_i \Phi_{kac} \partial_j \Phi_{lbd} \right). \quad (52)$$

The constraints of the Einstein evolution system used to construct \mathcal{C}_ψ are defined in Eqs. (19), (27), (38), (39), and (40). The dimensionless ratio between the norms of \mathcal{C}_ψ and \mathcal{N}_ψ is designed to give a meaningful measure of the fractional errors due to constraint violations of the Einstein system. The quantities \mathcal{C}_ϕ and \mathcal{N}_ϕ , defined by

$$\mathcal{C}_\phi^2 \equiv m^{ij} \left(\mathcal{C}_i^\phi \mathcal{C}_j^\phi + \frac{1}{2} m^{kl} \mathcal{C}_{ik}^\phi \mathcal{C}_{jl}^\phi \right), \quad (53)$$

$$\mathcal{N}_\phi^2 \equiv \mu^2 |\phi|^2, \quad (54)$$

play analogous roles for the Klein-Gordon evolution system. The scalar field constraints \mathcal{C}_i^ϕ and \mathcal{C}_{ij}^ϕ used to construct \mathcal{C}_ϕ are defined by $\mathcal{C}_i^\phi = \Phi_i^\phi - \tilde{\nabla}_i \phi$ and $\mathcal{C}_{ij}^\phi = \tilde{\nabla}_i \Phi_j^\phi - \tilde{\nabla}_j \Phi_i^\phi$.

Figures 1 and 2 show that our numerical solutions diverge exponentially away from the Einstein-Klein-Gordon static universe solution, while Fig. 3 shows that the constraints are well satisfied during a time in which

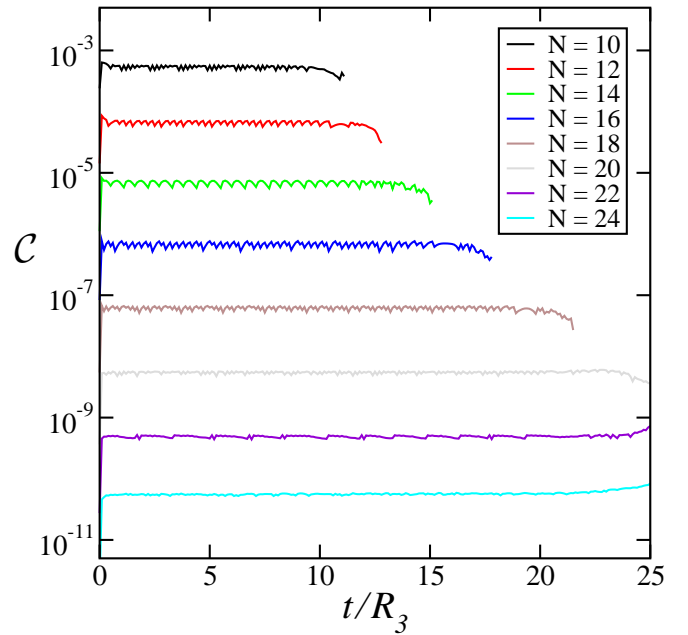


FIG. 3: Constraint norm \mathcal{C} in the numerical evolutions using initial data for the Einstein-Klein-Gordon static solution. Numerical resolution used in each spatial dimension of each cubic region is denoted by N .

this instability grows by over 10 orders of magnitude. Our numerical evolutions therefore confirm the existence of the instability of the Einstein static universe first noted by Eddington [3]. The growth rate of this instability can be measured numerically from our evolutions, giving $1/\tau_N \approx 1.100501(1)$, where the number in parentheses represents the estimated uncertainty in the last digit. This agrees with the analytical value, $1/\tau_A = \sqrt{2\sqrt{13} - 6} \approx 1.1005010$, computed for this unstable mode in Sec. VI.

V. MODE DAMPING

The straightforward numerical test of the Einstein-Klein-Gordon evolution system described in Sec. IV confirms that our implementation of the multicube method is basically correct and that our numerical methods are basically stable and convergent. Unfortunately, those evolutions persist for just a few light-crossing times of the S^3 geometry. These first tests do not, therefore, allow us to identify more subtle errors that might become evident only on much longer time scales. Nor do they test our implementation on solutions having more complicated spatial and temporal structures than the spatially homogeneous Einstein-Klein-Gordon static universe. We address these shortcomings in the following sections by performing more challenging variations on our original Einstein-Klein-Gordon static universe test.

In this section we construct small, unphysical damping forces that suppress the growth of the modes responsible

for the Eddington instability. The modified evolution equations can be written abstractly in the form

$$\partial_t \psi_{ab} = f_{ab} + \mathcal{D}f_{ab}, \quad (55)$$

$$\partial_t \Pi_{ab} = F_{ab} + \mathcal{D}F_{ab}, \quad (56)$$

$$\partial_t \phi = f_\phi + \mathcal{D}f_\phi, \quad (57)$$

$$\partial_t \Pi_\varphi = F_\phi + \mathcal{D}F_\phi, \quad (58)$$

where f_{ab} , F_{ab} , f_ϕ and F_ϕ are the expressions for the right sides of the unmodified Einstein-Klein-Gordon evolution equations, while $\mathcal{D}f_{ab}$, $\mathcal{D}F_{ab}$, $\mathcal{D}f_\phi$ and $\mathcal{D}F_\phi$ represent the unphysical mode-damping forces.

Any physical mode, in particular the one responsible for the Eddington instability, has a certain very specific spatial structure. This fact is used in this section to construct mode-damping forces that suppress the degrees of freedom of the system having that particular structure, while leaving unaffected the other dynamical degrees of freedom of the system. The effectiveness of the resulting mode-damping forces is then tested by evolving initial data for the Einstein-Klein-Gordon static universe solution. These tests confirm the effectiveness of these mode-damping forces. More importantly, these tests also confirm the numerical stability and convergence of our implementation of the multicube method for solving Einstein's equation over very long time scales.

The most convenient and efficient way to represent the spatial structures of tensor fields on S^3 is to expand those fields in the tensor harmonics of the three-sphere [21]. The basic properties of the scalar, vector, and rank-2 tensor three-sphere harmonics that are relevant to our work here are summarized in Appendix B. The particular harmonics that play an important role in the unstable modes of the Einstein-Klein-Gordon static universe are the scalar harmonics $Y^{k\ell m}$ and the vector harmonics $\tilde{\nabla}_i Y^{k\ell m}$. The time-dependent projections of a scalar field $Q(\vec{x}, t)$ and a vector field $V_i(\vec{x}, t)$ onto these harmonics are defined, respectively, as

$$Q^{k\ell m}(t) = \int Q(\vec{x}, t) Y^{*k\ell m} \sqrt{\tilde{g}} d^3x, \quad (59)$$

$$V^{k\ell m}(t) = \int \tilde{g}^{ij} V_i(\vec{x}, t) \tilde{\nabla}_j Y^{*k\ell m} \sqrt{\tilde{g}} d^3x, \quad (60)$$

where $Y^{*k\ell m}$ in these equations denotes the complex conjugate.

The mode responsible for the Eddington instability is spatially homogeneous, like the Einstein-Klein-Gordon solution itself. Therefore, the spatial structures of the dynamical fields for this mode are completely described by the $k = \ell = m = 0$ three-sphere harmonics. The mode-damping forces needed to suppress the growth of this instability can therefore be constructed using only the $k = \ell = m = 0$ three-sphere harmonic projections of the quantities $\psi = \tilde{g}^{ij} \psi_{ij}$, $f = \tilde{g}^{ij} f_{ij}$, ψ_{tt} , f_{tt} , $\Pi = \tilde{g}^{ij} \Pi_{ij}$, $F = \tilde{g}^{ij} F_{ij}$, Π_{tt} , F_{tt} , ϕ , f_ϕ , Π_ϕ , and F_ϕ . We use these three-sphere harmonic projections to construct the fol-

lowing mode-damping forces:

$$\begin{aligned} \mathcal{D}f_{ab}^{000} &\equiv -\frac{Y^{000}}{3R_3^3} \{f^{000}(t) + \eta_G [\psi^{000}(t) - \psi^{000}(0)]\} \tilde{g}_{ab} \\ &\quad - \frac{Y^{000}}{R_3^3} \{f_{tt}^{000}(t) + \eta_G [\psi_{tt}^{000}(t) - \psi_{tt}^{000}(0)]\} \hat{t}_a \hat{t}_b, \end{aligned} \quad (61)$$

$$\begin{aligned} \mathcal{D}F_{ab}^{000} &\equiv -\frac{Y^{000}}{3R_3^3} [F^{000}(t) + \eta_G \Pi^{000}(t)] \tilde{g}_{ab} \\ &\quad - \frac{Y^{000}}{R_3^3} [F_{tt}^{000}(t) + \eta_G \Pi_{tt}^{000}(t)] \hat{t}_a \hat{t}_b, \end{aligned} \quad (62)$$

$$\begin{aligned} \mathcal{D}f_\phi^{000} &\equiv -\frac{Y^{000}}{R_3^3} \{[f_\phi^{000}(t) - i\mu\phi^{000}(0)e^{i\mu t}] \\ &\quad + \eta_S [\phi^{000}(t) - \phi^{000}(0)e^{i\mu t}]\}, \end{aligned} \quad (63)$$

$$\begin{aligned} \mathcal{D}F_\phi^{000} &\equiv -\frac{Y^{000}}{R_3^3} \{[F_\phi^{000}(t) - i\mu\Pi_\phi^{000}(0)e^{i\mu t}] \\ &\quad + \eta_S [\Pi_\phi^{000}(t) - \Pi_\phi^{000}(0)e^{i\mu t}]\}, \end{aligned} \quad (64)$$

where $\hat{t}_a = \partial_a t$. The constants η_G and η_S in these equations are damping rates (of order unity) that control how quickly the mode damping acts to drive the $k = \ell = m = 0$ component of these solutions back toward their equilibrium values.

It is straightforward to show that the modified Einstein-Klein-Gordon evolution equations suppress the dynamics of the $k = \ell = m = 0$ degrees of freedom of the system, without affecting the dynamics in any other mode. Multiplying Eqs. (55)–(58) by Y^{*000} and integrating the scalar parts (i.e., the spatial trace and the tt components) over the S^3 geometry results in the following equations for the $k = \ell = m = 0$ components of the various dynamical fields:

$$\begin{aligned} \partial_t [\psi^{000}(t) - \psi^{000}(0)] &= \\ &\quad -\eta_G [\psi^{000}(t) - \psi^{000}(0)], \end{aligned} \quad (65)$$

$$\begin{aligned} \partial_t [\psi_{tt}^{000}(t) - \psi_{tt}^{000}(0)] &= \\ &\quad -\eta_G [\psi_{tt}^{000}(t) - \psi_{tt}^{000}(0)], \end{aligned} \quad (66)$$

$$\partial_t \Pi^{000}(t) = -\eta_G \Pi^{000}(t), \quad (67)$$

$$\partial_t \Pi_{tt}^{000}(t) = -\eta_G \Pi_{tt}^{000}(t), \quad (68)$$

$$\begin{aligned} \partial_t [\phi^{000}(t) - \phi^{000}(0)e^{i\mu t}] &= \\ &\quad -\eta_S [\phi^{000}(t) - \phi^{000}(0)e^{i\mu t}], \end{aligned} \quad (69)$$

$$\begin{aligned} \partial_t [\Pi_\varphi^{000}(t) - \Pi_\varphi^{000}(0)e^{i\mu t}] &= \\ &\quad -\eta_S [\Pi_\varphi^{000}(t) - \Pi_\varphi^{000}(0)e^{i\mu t}]. \end{aligned} \quad (70)$$

These equations drive the $k = \ell = m = 0$ components of the various dynamical fields toward their initial values.

Initial data for the Klein-Gordon static universe solution have been evolved with the modified equations that include the $k = \ell = m = 0$ mode-damping forces defined in Eqs. (61)–(64). Unfortunately, the resulting evolutions are still unstable. The numerically determined growth rate of this new instability is $1/\tau_{\mathcal{N}} \approx 0.6180(1)$, where

the number in parentheses represents the estimated uncertainty in the last digit. This agrees with the analytical value, $1/\tau_{\mathcal{A}} = (\sqrt{4 + \mu_G^2 R_3^2} - \mu_G R_3)/2 = (\sqrt{5} - 1)/2 \approx 0.618034$, computed for an unstable $k = 1$ mode of this system in Sec. VI. The growth rate of this new unstable mode is set by the constant μ_G (taken to have the value $\mu_G = 1/R_3$ in our numerical tests) that controls the gauge condition, Eq. (47), used in our evolutions. The modes responsible for this somewhat weaker gauge instability have spatial structures determined by the various $k = 1$ three-sphere harmonics. This instability can also be suppressed, therefore, by constructing the appropriate $k = 1$ mode-damping forces.

The $k = 1$ parts of the Einstein-Klein-Gordon static solution have $0 = \psi^{1\ell m}(t) = f^{1\ell m}(t) = \psi_{tt}^{1\ell m}(t) = f_{tt}^{1\ell m}(t) = \psi_{tj}^{1\ell m}(t) = f_{tj}^{1\ell m}(t) = \phi^{1\ell m}(t) = f_{\phi}^{1\ell m}(t)$. The evolution equations can therefore be modified to drive the dynamical solution toward the state having no $k = 1$ three-sphere harmonic content by adding the following mode-damping forces:

$$\begin{aligned} \mathcal{D}f_{ab}^{1\ell m} \equiv & -\frac{Y^{1\ell m}}{3R_3^3} [f^{1\ell m}(t) + \eta_G \psi^{1\ell m}(t)] \tilde{g}_{ab} \\ & -\frac{\hat{t}_a \tilde{\nabla}_b Y^{1\ell m} + \hat{t}_b \tilde{\nabla}_a Y^{1\ell m}}{3R_3} [f_{tj}^{1\ell m}(t) + \eta_G \psi_{tj}^{1\ell m}(t)], \\ & -\frac{Y^{1\ell m}}{R_3^3} [f_{tt}^{1\ell m}(t) + \eta_G \psi_{tt}^{1\ell m}(t)] \hat{t}_a \hat{t}_b, \end{aligned} \quad (71)$$

$$\mathcal{D}f_{\phi}^{1\ell m} \equiv -\frac{Y^{1\ell m}}{R_3^3} [f_{\phi}^{1\ell m}(t) + \eta_S \phi^{k\ell m}(t)]. \quad (72)$$

Similar forces could be constructed to suppress the $k = 1$ dynamics in the evolution equations for Π_{ab} and Π_{ϕ} . Such forces are not needed to control the growth of this rather weak $k = 1$ instability, however, so a minimalist approach has been followed by setting $0 = \mathcal{D}F_{ab}^{1\ell m} = \mathcal{D}F_{\phi}^{1\ell m}$.

Combining the $k = 0$ damping forces from Eqs. (61)–(64) with the $k = 1$ forces from Eqs. (71) and (72) gives the needed composite mode-damping forces:

$$\mathcal{D}f_{ab} = \mathcal{D}f_{ab}^{000} + \sum_{\ell=0}^1 \sum_{m=-\ell}^{\ell} \mathcal{D}f_{ab}^{1\ell m}, \quad (73)$$

$$\mathcal{D}F_{ab} = \mathcal{D}F_{ab}^{000}, \quad (74)$$

$$\mathcal{D}f_{\phi} = \mathcal{D}f_{\phi}^{000} + \sum_{\ell=0}^1 \sum_{m=-\ell}^{\ell} \mathcal{D}f_{\phi}^{1\ell m}, \quad (75)$$

$$\mathcal{D}F_{\phi} = \mathcal{D}F_{\phi}^{000}. \quad (76)$$

The resulting modified Einstein-Klein-Gordon evolution system suppresses the dynamics in the $k = 0$ three-sphere harmonic components of ψ_{ab} , Π_{ab} , ϕ and Π_{ϕ} according to Eqs. (65)–(70). In addition, the modified system also suppresses the dynamics in the $k = 1$ three-sphere har-

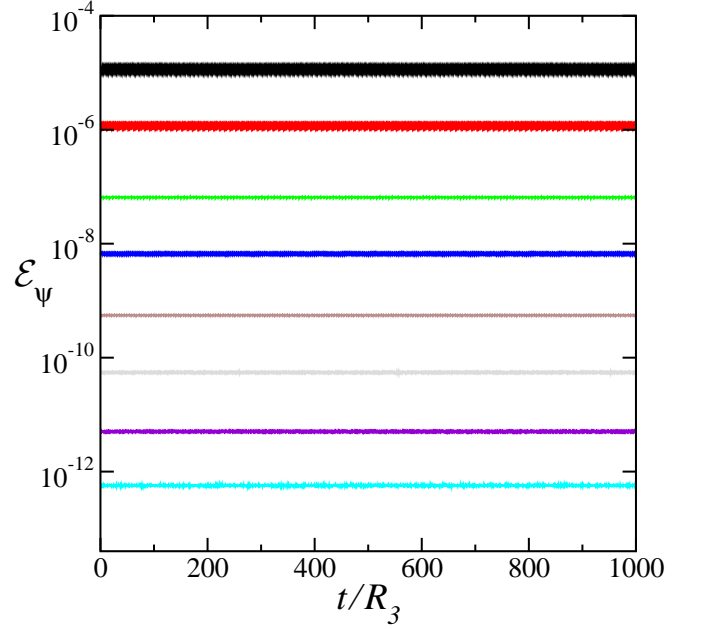


FIG. 4: Errors in the metric ψ_{ab} for evolutions (including mode-damping forces) of initial data for the Einstein-Klein-Gordon static solution. Numerical resolutions are the same as those shown in Figs. 1–3.

monic components ψ_{ab} and ϕ in the following way:

$$\partial_t \psi_{tt}^{1\ell m}(t) = -\eta_G \psi_{tt}^{1\ell m}(t), \quad (77)$$

$$\partial_t \psi_{tj}^{1\ell m}(t) = -\eta_G \psi_{tj}^{1\ell m}(t), \quad (78)$$

$$\partial_t \psi^{1\ell m}(t) = -\eta_G \psi^{1\ell m}(t), \quad (79)$$

$$\partial_t \phi^{1\ell m}(t) = -\eta_S \phi^{1\ell m}(t). \quad (80)$$

The second numerical test of our implementation of the multicube method evolves the coupled Einstein and Klein-Gordon evolution equations, modified with the $k = 0$ and $k = 1$ mode-damping forces. The initial data used for these evolutions are those of the static Einstein-Klein-Gordon universe solution, described in detail in Sec. IV. Figures 4 and 5 illustrate the errors in the metric ψ_{ab} and the Klein-Gordon scalar field ϕ , as measured by the quantities \mathcal{E}_{ψ} and \mathcal{E}_{ϕ} defined in Eqs. (48) and (49), respectively. Figure 6 illustrates the constraint norm \mathcal{C} defined in Eq. (54) for this test. These results show that the mode-damping forces are effective in suppressing the $k = 0$ and the $k = 1$ instabilities that appeared in our earlier tests. The light-crossing time of the S^3 geometry is $2\pi R_3$, so these results demonstrate numerical stability and convergence for about 160 light-crossing times of the solution.

The results shown in Figs. 4–6 demonstrate that the constraints of the Einstein-Klein-Gordon evolution system are satisfied, and that the numerical solution converges to the Einstein-Klein-Gordon static universe solution. These results do not demonstrate, however, that the physical Einstein-Klein-Gordon equations are actually satisfied. The mode-damping forces, $\mathcal{D}f_{ab}$, $\mathcal{D}F_{ab}$,

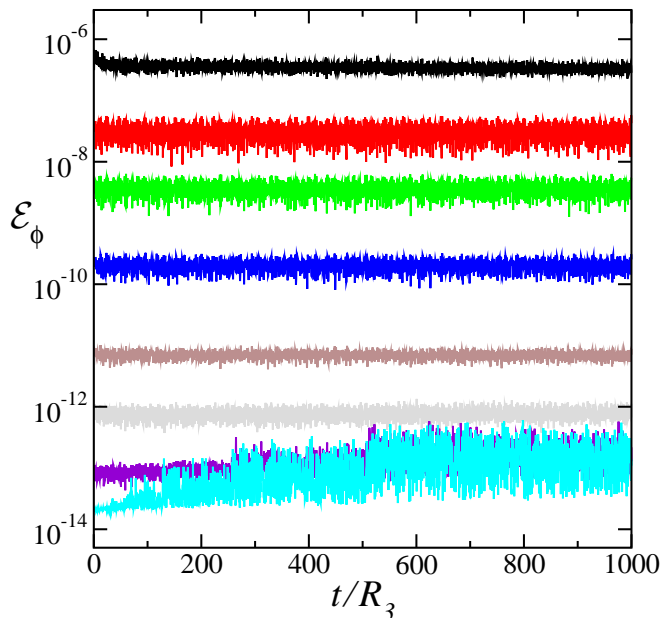


FIG. 5: Errors in the complex Klein-Gordon scalar field ϕ for evolutions (including mode-damping forces) of initial data for the Einstein-Klein-Gordon static solution. Numerical resolutions are the same as those shown in Figs. 1–3.

$\mathcal{D}f_\phi$, and $\mathcal{D}F_\phi$ must be measured to confirm that. We measure the sizes of these mode-damping forces with the quantity $\mathcal{E}_\mathcal{D}$, defined as the integral norm of each component of each mode-damping force:

$$\mathcal{E}_\mathcal{D}^2 \equiv \frac{\int m^{ab}m^{cd} \mathcal{D}f_{ac} \mathcal{D}f_{bd} \sqrt{g} d^3x}{\int \mu^2 m^{ab}m^{cd} \psi_{ac}\psi_{bd} \sqrt{g} d^3x} + \frac{\int m^{ab}m^{cd} \mathcal{D}F_{ac} \mathcal{D}F_{bd} \sqrt{g} d^3x}{\int \mu^4 m^{ab}m^{cd} \psi_{ac}\psi_{bd} \sqrt{g} d^3x} + \frac{\int |\mathcal{D}f_\phi|^2 \sqrt{g} d^3x}{\int \mu^2 |\phi|^2 \sqrt{g} d^3x} + \frac{\int |\mathcal{D}F_\phi|^2 \sqrt{g} d^3x}{\int \mu^4 |\phi|^2 \sqrt{g} d^3x}. \quad (81)$$

The factors of μ (the fundamental scalar field oscillation frequency) in this expression are used as characteristic time scales in the denominators to make $\mathcal{E}_\mathcal{D}$ dimensionless. Figure 7 shows that the mode-damping forces converge to zero as the numerical resolution is increased, so our numerical solution also solves the unmodified *physical* Einstein-Klein-Gordon evolution equations in this limit. Consequently, the results shown in Figs. 4–7 demonstrate that our implementation of the multicube method for solving Einstein’s equation on manifolds with nontrivial spatial topologies is stable and numerically convergent even for very long-time-scale evolutions.

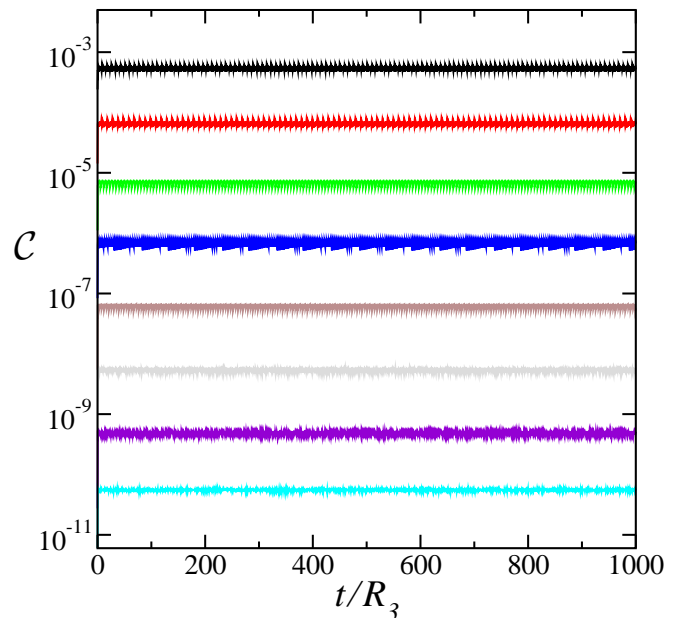


FIG. 6: Constraint norm \mathcal{C} for evolutions (including mode-damping forces) of initial data for the Einstein-Klein-Gordon static solution. Numerical resolutions are the same as those shown in Figs. 1–3.

VI. PERTURBED EINSTEIN-KLEIN-GORDON STATIC UNIVERSE

The numerical tests of the Einstein-Klein-Gordon evolution system described in Sec. V confirm that our implementation of the multicube method for solving Einstein’s equation described in Secs. II and III is basically correct and free of numerical instabilities even on rather long time scales. Those numerical tests were limited, however, by the fact that the Einstein-Klein-Gordon static universe solution is time independent and its spatial structure is extremely simple. In this section we address these limitations by carrying out a third, more challenging, set of numerical tests of the multicube methods by performing long-time-scale evolutions of complicated time-dependent perturbations of the Einstein-Klein-Gordon static universe solution. We study these perturbed solutions analytically in Sec. VIA and numerically in Sec. VIB. The results demonstrate that our numerical nonlinear Einstein-Klein-Gordon code successfully evolves complicated dynamical solutions having significant spatial structures. We show that these numerical solutions converge to solutions of the Einstein-Klein-Gordon evolution system that agree with the analytical predictions.

A. Analytical perturbations

In this section we derive analytically the general solutions to the coupled Einstein and Klein-Gordon equa-

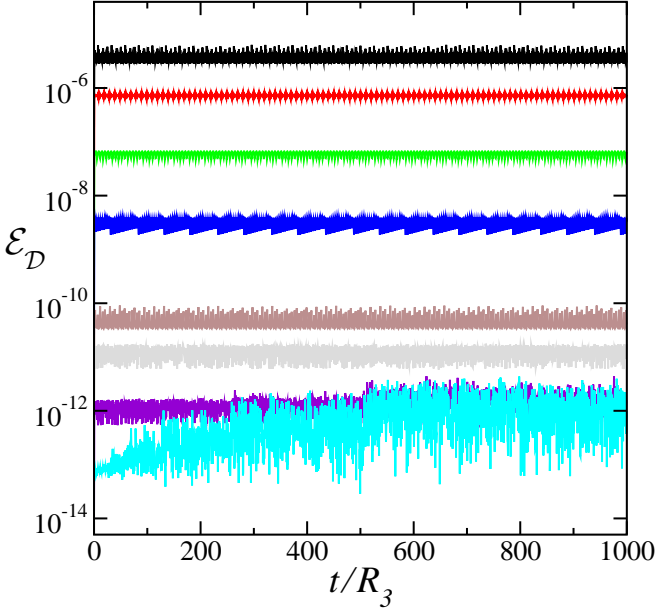


FIG. 7: Norm of the mode-damping forces, \mathcal{E}_D , for evolutions (including mode-damping forces) of initial data for the Einstein-Klein-Gordon static solution. Numerical resolutions are the same as those shown in Figs. 1–3.

tions for perturbations about the Einstein-Klein-Gordon static universe solution. Write the spacetime metric ψ_{ab} and the scalar field ϕ for this perturbed solution as

$$\psi_{ab} = \psi_{ab}^0 + \delta\psi_{ab}, \quad (82)$$

$$\phi = \phi_0 e^{i\mu t} + \delta\phi, \quad (83)$$

where ψ_{ab}^0 and $\phi_0 e^{i\mu t}$ are the “background” metric and scalar fields of the Einstein-Klein-Gordon static universe solution. The background metric ψ_{ab}^0 is identical to the reference metric $\tilde{\psi}_{ab}$ used to fix the differential structure in our multicube representation of S^3 . We will therefore refer to the background metric as $\tilde{\psi}_{ab}$. The evolution equations for the perturbations, $\delta\psi_{ab}$ and $\delta\phi$, are obtained by linearizing the coupled Einstein-Klein-Gordon equations about this background. The perturbed Ricci tensor is given by

$$\begin{aligned} \delta R_{ab} = & -\frac{1}{2}\tilde{\nabla}^c\tilde{\nabla}_c\delta\psi_{ab} - \tilde{\nabla}_{(a}\delta H_{b)} + \frac{2}{R_3^2}\tilde{g}^c{}_{(a}\delta\psi_{b)c} \\ & -\frac{1}{R_3^2}(\tilde{g}^{cd}\tilde{g}_{ab} - \tilde{g}^c{}_{(a}\tilde{g}^d{}_{b)})\delta\psi_{cd}, \end{aligned} \quad (84)$$

where $\tilde{\nabla}_a$ is the covariant derivative associated with the background metric $\tilde{\psi}_{ab}$, and $\tilde{g}_{ab} = \tilde{\psi}_{ab} + \tilde{\nabla}_a t \tilde{\nabla}_b t$ is the background spatial metric. The perturbed Einstein equation is given by

$$\delta R_{ab} = (\Lambda - 4\pi T_0)\delta\psi_{ab} + 8\pi\left(\delta T_{ab} - \frac{1}{2}\tilde{\psi}_{ab}\delta T\right), \quad (85)$$

where $\Lambda = 1/R_3^2$ and $4\pi T_0 = -1/R_3^2$ are the cosmological constant and trace of the stress tensor from

the background spacetime, respectively, and δT_{ab} and $\delta T = \tilde{\psi}^{ab}\delta T_{ab} - T_0^{ab}\delta\psi_{ab}$ are the perturbed stress-energy tensor and its trace. For the Einstein-Klein-Gordon system, the perturbed stress-energy tensor is given by

$$\begin{aligned} \delta T_{ab} - \frac{1}{2}\tilde{\psi}_{ab}\delta T = & \frac{1}{2}\mu^2(\phi_0 e^{i\mu t}\delta\phi^* + \phi_0^* e^{-i\mu t}\delta\phi)\tilde{\psi}_{ab} \\ & + i\mu\phi_0 e^{i\mu t}\tilde{\nabla}_{(a}\delta\phi^*\tilde{\nabla}_{b)}t - i\mu\phi_0^* e^{-i\mu t}\tilde{\nabla}_{(a}\delta\phi\tilde{\nabla}_{b)}t. \end{aligned} \quad (86)$$

The perturbed Klein-Gordon equation for this system is given by

$$0 = \tilde{\nabla}^a\tilde{\nabla}_a\delta\phi - \mu^2\delta\phi + \mu^2\phi_0 e^{i\mu t}\delta\psi_{tt}. \quad (87)$$

The perturbed damped harmonic gauge condition for this system is given by

$$0 = \tilde{\nabla}^b\delta\psi_{ba} - \frac{1}{2}\tilde{\psi}^{bc}\tilde{\nabla}_a\delta\psi_{bc} - \mu_G\tilde{g}_a{}^b\delta\psi_{bt}. \quad (88)$$

The perturbations of the Einstein-Klein-Gordon static solution are determined by solving the linearized system, Eqs. (84)–(88), for $\delta\psi_{ab}$ and $\delta\phi$.

These perturbed Einstein-Klein-Gordon equations can be decoupled into separate equations for the scalar, vector, and tensor degrees of freedom of the system. To accomplish this, the perturbed metric $\delta\psi_{ab}$ is decomposed into two scalars (under spatial coordinate transformations) $\delta\psi_{tt}$ and $\delta\psi = \tilde{\psi}^{ij}\delta\psi_{ij}$, one vector $\delta\psi_{jt}$, and one trace-free tensor $\delta\bar{\psi}_{ij} = \delta\psi_{ij} - \frac{1}{3}\tilde{\psi}_{ij}\delta\psi$. These fields can then be represented as linear combinations of the appropriate scalar, vector, and tensor harmonics on the three-sphere (as described in Appendix B). Since the background Einstein-Klein-Gordon solution is static, the solutions to the perturbation equations can be expressed as linear combinations of modes, i.e., solutions having time dependence $e^{i\omega t}$.

We first discuss the modes corresponding to the scalar degrees of freedom of the system. The perturbations of $\delta\psi_{ab}$ and $\delta\phi$ for a general scalar mode can be written in the form

$$\delta\psi_{tt} = \Re[A_{tt}Y^{klm}e^{i\omega st}], \quad (89)$$

$$\delta\psi_{tj} = \Im[A_{tj}Y_{(0)j}^{klm}e^{i\omega st}], \quad (90)$$

$$\delta\psi = \Re[A_{\psi}Y^{klm}e^{i\omega st}], \quad (91)$$

$$\delta\bar{\psi}_{jk} = \Im[A_{\bar{j}\bar{k}}Y_{(3)jk}^{klm}e^{i\omega st}], \quad (92)$$

$$\delta\phi = \phi_0 e^{i\mu t}\left[A_{\phi}^+Y^{klm}e^{i\omega st} + A_{\phi}^{-*}Y^{klm*}e^{-i\omega st}\right], \quad (93)$$

where A_{tt} , A_{tj} , A_{ψ} , $A_{\bar{j}\bar{k}}$, A_{ϕ}^+ , and A_{ϕ}^- are complex constants; Y^{klm} , $Y_{(0)j}^{klm}$, and $Y_{(3)jk}^{klm}$ are the scalar, vector, and tensor harmonics on S^3 defined in Appendix B; ω_S is the frequency of the mode; and $\Re(Z)$ and $\Im(Z)$ denote the real and imaginary parts of a quantity Z , respectively. The perturbed Einstein-Klein-Gordon equations for these perturbations become a system of linear algebraic equations for the amplitudes A_{tt} , \dots . These linear equations have solutions whenever the frequency ω_S

is one of the mode eigenfrequencies of the system. For these values of ω_S the general solution to the perturbation equations can be written as

$$A_{tt} = A_S^{k\ell m}, \quad (94)$$

$$A_\psi = -A_S^{k\ell m} - \frac{16k(k+2)\mu^2 R_3^2}{Q} A_S^{k\ell m}, \quad (95)$$

$$A_\phi^+ = -\frac{\mu^2 R_3^2}{2[\omega_S(\omega_S + 2\mu)R_3^2 - k(k+2)]} A_S^{k\ell m}, \quad (96)$$

$$A_\phi^- = -\frac{\mu^2 R_3^2}{2[\omega_S(\omega_S - 2\mu)R_3^2 - k(k+2)]} A_S^{k\ell m}, \quad (97)$$

$$A_{tj} = -\frac{8\mu^2 \omega_S R_3^4}{Q} A_S^{k\ell m}, \quad (98)$$

$$A_{j\bar{k}} = -\frac{16\mu_G \mu^2 \omega_S R_3^6}{Q[\omega_S^2 R_3^2 + 4 - k(k+2)]} A_S^{k\ell m}, \quad (99)$$

where $A_S^{k\ell m}$ is the complex constant that sets the amplitude of the scalar mode, and Q is defined by

$$Q = [\omega_S(\omega_S - i\mu_G)R_3^2 + 4 - k(k+2)] \times \{[\omega_S^2 R_3^2 - k(k+2)]^2 - 4\mu^2 \omega_S^2 R_3^4\}. \quad (100)$$

The allowed eigenfrequencies of these modes break up into three distinct families, defined by

$$(\omega_S^0 R_3)^2 = k(k+2), \quad (101)$$

$$(\omega_S^\pm R_3)^2 = k(k+2) + 2(\mu^2 R_3^2 - 1) \pm 2\sqrt{(\mu^2 R_3^2 - 1)^2 + [k(k+2) + 1]\mu^2 R_3^2}. \quad (102)$$

It is straightforward to show that $(\omega_S^\pm R_3)^2 > 0$ when $k \geq 2$ and $8 \geq \mu^2 R_3^2$, so the generic scalar modes are stable in these cases.

The scalar modes for the cases $k = 0$ and $k = 1$ are somewhat exceptional and must be calculated separately. For the $k = 0$ case, the vector and tensor harmonics, $Y_{(0)j}^{k\ell m}$ and $Y_{(3)ij}^{k\ell m}$, both vanish, so the mode amplitudes A_{tj} and $A_{j\bar{k}}$ are effectively zero. The mode amplitudes of the remaining scalar degrees of freedom, A_{tt} , A_ψ , A_ϕ^+ , and A_ϕ^- , are given by the expressions in Eqs. (94)–(97) with $k = 0$, but there are only two independent mode frequencies in this case:

$$(\omega_S^\pm R_3)^2 = 2\mu^2 R_3^2 - 2 \pm 2\sqrt{\mu^4 R_3^4 - \mu^2 R_3^2 + 1}. \quad (103)$$

One of these has an imaginary frequency, $(\omega_S^- R_3)^2 < 0$, and therefore represents an unstable mode of the Einstein-Klein-Gordon system. The instability seen in the numerical evolution discussed in Sec. IV has a growth rate that matches with great accuracy the analytical rate predicted by this unstable $k = 0$ mode frequency, ω_S^- . There is also a degenerate exceptional $k = 0$ mode having $\omega_S R_3 = 0$. This mode has $A_{tt} = A_\psi = 0$ and $A_\phi^+ = -A_\phi^-$. This exceptional mode does not excite the gravitational field at all and appears to be a kind of gauge mode associated with the phase of the complex scalar field ϕ .

The other exceptional scalar modes are those with $k = 1$. In this case the tensor harmonics $Y_{(3)ij}^{k\ell m}$ vanish identically, so in effect $A_{j\bar{k}} = 0$. Repeating the mode calculation gives the expressions in Eqs. (94)–(98) with $k = 1$. There are, however, a smaller number of mode frequencies in this case:

$$(\omega_S^\pm R_3)^2 = 3 + 2\mu^2 R_3^2 \pm 2\mu^2 R_3^2,$$

both of which satisfy $(\omega_S^\pm R_3)^2 > 0$ and are therefore stable. In addition, there are two other $k = 1$ modes that have somewhat different mode structures. For these modes,

$$A_{tt} = A_\phi^+ = A_\phi^- = 0, \quad (104)$$

$$A_\psi = 6(\omega_S - i\mu_G)R_3 A_S^{k\ell m}, \quad (105)$$

$$A_{tj} = A_S^{k\ell m}. \quad (106)$$

The frequencies of these exceptional $k = 1$ modes are given by

$$\omega_S^\pm R_3 = \frac{i}{2} \left(\mu_G R_3 \pm \sqrt{4 + \mu_G^2 R_3^2} \right). \quad (107)$$

One of these modes is a nonoscillatory damped mode, while the other mode is unstable. The instability seen in the preliminary numerical evolution discussed in Sec. V has a growth rate that matches the analytical rate predicted by this ($k = 1$)-mode frequency ω_S^- . This exceptional $k = 1$ mode does not excite the Klein-Gordon scalar field at all and appears to be associated with the coordinate gauge freedom of the gravitational field.

The Einstein-Klein-Gordon perturbation equations also admit mode solutions that represent the vector degrees of freedom of the gravitational field. The modes representing these vector degrees of freedom can be written quite generally as

$$\delta\psi_{tj} = \Re \left\{ i\omega_V \left[A_{V(1)}^{k\ell m} Y_{(1)j}^{k\ell m} + A_{V(2)}^{k\ell m} Y_{(2)j}^{k\ell m} \right] e^{i\omega_V t} \right\}, \quad (108)$$

$$\delta\bar{\psi}_{jk} = \Re \left\{ 2 \left[A_{V(1)}^{k\ell m} Y_{(1)jk}^{k\ell m} + A_{V(2)}^{k\ell m} Y_{(2)jk}^{k\ell m} \right] e^{i\omega_V t} \right\}. \quad (109)$$

Here, $A_{V(1)}^{k\ell m}$ and $A_{V(2)}^{k\ell m}$ are (complex) constants; and $Y_{(1)j}^{k\ell m}$, $Y_{(2)j}^{k\ell m}$, $Y_{(1)jk}^{k\ell m}$, and $Y_{(2)jk}^{k\ell m}$ are the type-1 and type-2 vector and tensor harmonics defined in Eqs. (B3), (B4), (B12), and (B13) in Appendix B. These harmonics are defined only for $k \geq 1$. The perturbed Einstein-Klein-Gordon equations admit solutions of this type for arbitrary values of the mode amplitudes, $A_{V(1)}^{k\ell m}$ and $A_{V(2)}^{k\ell m}$, whenever the frequency ω_V satisfies the vector-mode eigenfrequency condition

$$(\omega_V - i\mu_G/2)^2 R_3^2 = k(k+2) - 3 - \mu_G^2 R_3^2/4. \quad (110)$$

The quantity $\mu_G > 0$ that appears in these expressions is the harmonic gauge damping factor defined in Eq. (47). The frequencies of these modes are complex with non-negative imaginary parts, so these vector modes are all

stable. These vector modes appear to be associated with the spatial coordinate gauge degrees of freedom of the system.

Finally, there is a set of modes that represent the tensor degrees of freedom of the system. The two tensor degrees of freedom are the trace-free, $\delta\bar{\psi}_{jk} = \delta\psi_{jk} - \frac{1}{2}\psi_{0jk}\psi_0^{rs}\delta\psi_{rs}$, and transverse, $\nabla^k\delta\bar{\psi}_{jk} = 0$, parts of the metric perturbation. The general form for these tensor modes is given by

$$\delta\bar{\psi}_{jk} = \Re \left\{ \left[A_{T(4)}^{k\ell m} Y_{(4)jk}^{k\ell m} + A_{T(5)}^{k\ell m} Y_{(5)jk}^{k\ell m} \right] e^{i\omega_T t} \right\}, \quad (111)$$

where $A_{T(5)}^{k\ell m}$ and $A_{T(4)}^{k\ell m}$ are constants, and $Y_{(4)jk}^{k\ell m}$ and $Y_{(5)jk}^{k\ell m}$ are the type-4 and type-5 tensor harmonics defined in Eqs. (B15) and (B16) in Appendix B. These tensor harmonics exist only for $k \geq 2$ and $\ell \geq 2$. The perturbed Einstein-Klein-Gordon equations for these modes are satisfied for arbitrary (small) values of the complex constants $A_{T(5)}^{k\ell m}$ and $A_{T(4)}^{k\ell m}$, as long as the frequency ω_T satisfies the tensor-mode eigenfrequency condition

$$\omega_T^2 R_3^2 = k(k+2). \quad (112)$$

These frequencies are real, $\omega_T^2 R_3^2 > 0$, so the transverse-traceless tensor modes are all stable. These tensor modes correspond to the gravitational radiation degrees of freedom of the system.

We note that the modes of the Einstein-Klein-Gordon static universe found in these analytical solutions are all stable, except for two unstable modes. These unstable $k=0$ and $k=1$ modes correspond exactly to the unstable modes found in the numerical tests described in Secs. IV and V. This fact provides additional (indirect) evidence that our numerical implementation of the multicube method has been done correctly.

B. Numerical tests

The third numerical test of our implementation of the multicube method evolves initial data constructed from the analytical perturbation solutions of the coupled Einstein-Klein-Gordon evolution equations described in Sec. VI A. We define the analytical metric, ψ_{ab}^A , and scalar field, ϕ^A , solutions to be

$$\psi_{ab}^A = \tilde{\psi}_{ab} + \delta\psi_{ab}, \quad (113)$$

$$\phi^A = \phi_0 e^{i\mu t} + \delta\phi. \quad (114)$$

We construct the $\delta\psi_{ab}$ and $\delta\phi$ that appear in these definitions by taking linear combinations of the scalar mode solutions described in Eqs. (94)–(99). We include fifteen distinct scalar modes with spherical harmonic indices ranging from $k=2$ to $k=6$ and with a variety of values of the spherical harmonic indices ℓ and m . The amplitudes $A_S^{k\ell m}$ of the individual modes used to construct this solution are given in Table I. Also included in Table I is the choice of eigenfrequency class for each

mode, as defined in Eqs. (101) and (102). The amplitudes of these modes were chosen to be about 10^{-6} (or smaller) to ensure that the second-order (in amplitude) terms would be comparable to the double-precision round-off errors in our numerical evolutions. We chose this particular mix of harmonics to produce a solution having a complicated and interesting-looking dynamical evolution. Figure 8 illustrates the metric perturbation $\delta\psi_{tt}$ for this solution evaluated on the equatorial two-sphere, $\chi = \pi/2$, of the three-sphere geometry. The individual frames in Fig. 8 illustrate this field at times $t=0$, $t=6R_3$, and $t=12R_3$. These times (approximately one light-crossing time apart) do not correspond to any natural period of the system, and are intended to illustrate the complex, chaotic-looking dynamics produced by the chosen initial data.

We use the analytical fields ψ_{ab}^A and ϕ^A defined in Eqs. (113) and (114) to construct initial data for the Einstein-Klein-Gordon evolution system. We evolve these data numerically using the Einstein-Klein-Gordon equations that include the unphysical mode-damping forces defined in Eqs. (73)–(76). Figures 9 and 10 illustrate the differences between the numerically determined fields, ψ_{ab}^N and ϕ^N , and the analytical fields defined in Eqs. (113) and (114). These results show that the numerical solutions converge toward the analytical solutions until the size of their differences approaches 10^{-12} . The analytical fields were constructed from solutions to the first-order perturbation equations, and so they are expected to contain errors at this level of accuracy. Figures 11 and 12 show that the constraints of the Einstein-Klein-Gordon system as well as the unphysical mode-damping forces are numerically convergent (toward zero) in these evolutions. These tests provide strong additional evidence that our implementation of the multicube method for solving Einstein's equation described in Secs. II and III is correct and free from numerical instabilities.

TABLE I: Amplitudes and frequency classes of the individual modes of the perturbed Einstein-Klein-Gordon system used to form the analytic perturbation solution for the long-term stability tests shown in Figs. 9–12.

| k | ℓ | m | $A_S^{k\ell m}$ | ω_S | k | ℓ | m | $A_S^{k\ell m}$ | ω_S |
|-----|--------|-----|----------------------|--------------|-----|--------|-----|----------------------|--------------|
| 2 | 2 | 2 | 1.0×10^{-6} | ω_S^0 | 5 | 5 | 5 | 4.0×10^{-7} | ω_S^0 |
| 2 | 2 | -1 | 1.0×10^{-6} | ω_S^+ | 5 | 5 | 4 | 4.0×10^{-7} | ω_S^+ |
| 2 | 1 | 1 | 1.0×10^{-6} | ω_S^- | 5 | 4 | -3 | 4.0×10^{-7} | ω_S^- |
| 3 | 3 | -2 | 6.7×10^{-7} | ω_S^0 | 6 | 6 | 6 | 3.3×10^{-7} | ω_S^0 |
| 3 | 3 | 1 | 6.7×10^{-7} | ω_S^+ | 6 | 6 | -5 | 3.3×10^{-7} | ω_S^+ |
| 3 | 2 | 0 | 6.7×10^{-7} | ω_S^- | 6 | 5 | 3 | 3.3×10^{-7} | ω_S^- |
| 4 | 4 | -4 | 5.0×10^{-7} | ω_S^0 | | | | | |
| 4 | 4 | 3 | 5.0×10^{-7} | ω_S^+ | | | | | |
| 4 | 3 | -2 | 5.0×10^{-7} | ω_S^- | | | | | |

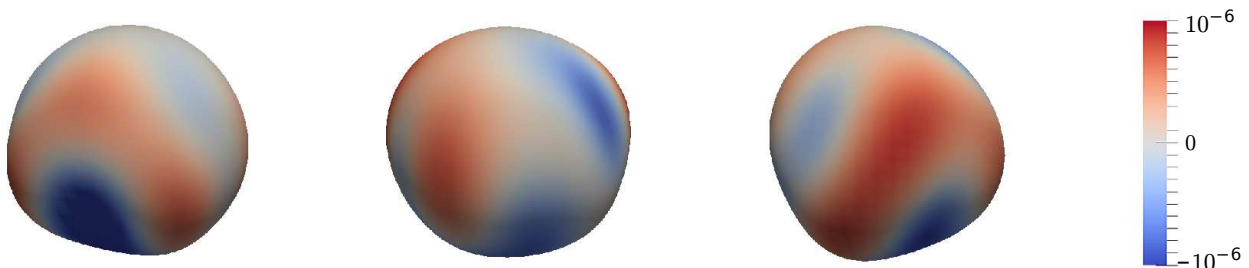


FIG. 8: Images of the $\delta\psi_{tt}$ component of the metric perturbation, evaluated on the equatorial two-sphere, $\chi = \pi/2$, of the perturbed Einstein-Klein-Gordon static solution. These images represent the times $t = 0$, $t = 6R_3$, and $t = 12R_3$. The color coding and distortion of the sphere represent the (scaled) magnitude of $\delta\psi_{tt}$.

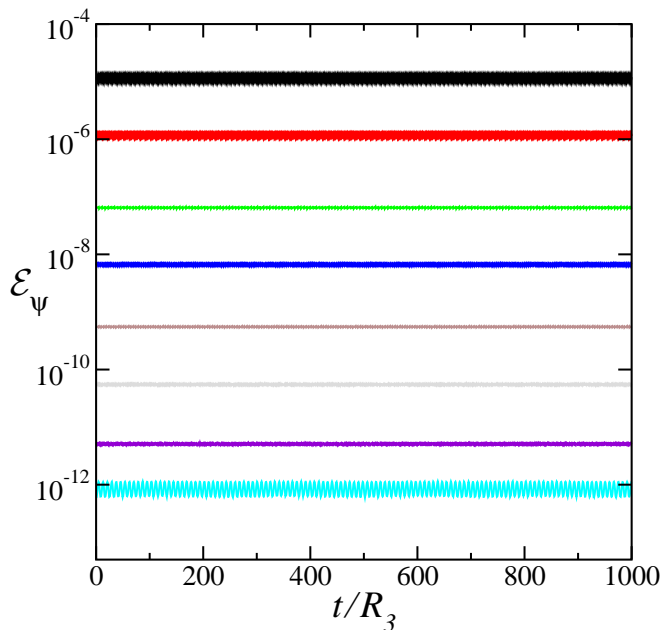


FIG. 9: Errors in the metric ψ_{ab} for evolutions (including mode-damping forces) of initial data for the perturbed Einstein-Klein-Gordon solution. Numerical resolutions are the same as those shown in Figs. 1–3.

VII. SUMMARY

In this paper we extend the multicube method for solving partial differential equations on manifolds with arbitrary spatial topologies, developed in Ref. [1], to allow us to solve Einstein’s equation on such manifolds. We accomplish this by developing in Sec. III a new spatially covariant first-order symmetric hyperbolic representation of Einstein’s equation. This new representation is equivalent to the standard noncovariant first-order generalized harmonic representations (e.g., Ref. [2]) on manifolds with spatial slices that can be embedded in R^3 . We test our implementation of these multicube methods in the SpEC code (developed by the SXS Collaboration, originally at Caltech and Cornell) in Sec. IV by evol-

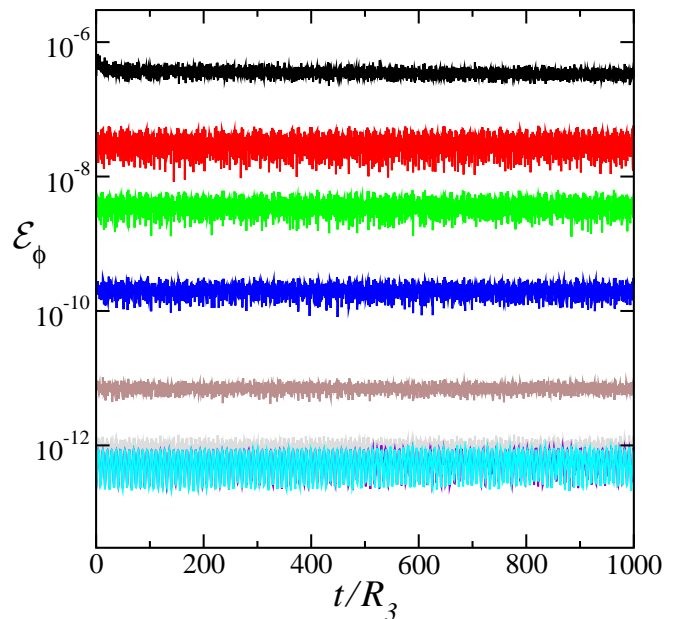


FIG. 10: Errors in the complex Klein-Gordon field ϕ for evolutions (including mode-damping forces) of initial data for the perturbed Einstein-Klein-Gordon solution. Numerical resolutions are the same as those shown in Figs. 1–3.

ing initial data for a new representation of the Einstein static universe metric on $R \times S^3$. Our representation uses a complex Klein-Gordon scalar field to provide the energy density for this spacetime. These numerical tests reproduce with great precision the well-known Eddington [3] instability of the Einstein static universe.

We have tested the accuracy and the long-time-scale numerical stability of our implementation of these multicube methods by adding unphysical damping forces to Einstein’s equation in Sec. V. These damping forces are designed to suppress the modes responsible for the Eddington instability and to leave all the other dynamical degrees of freedom of the system unchanged. These long-time-scale tests confirm stability and numerical convergence for about 160 light-crossing times of the S^3 geometry. Finally, we have derived analytical expressions for

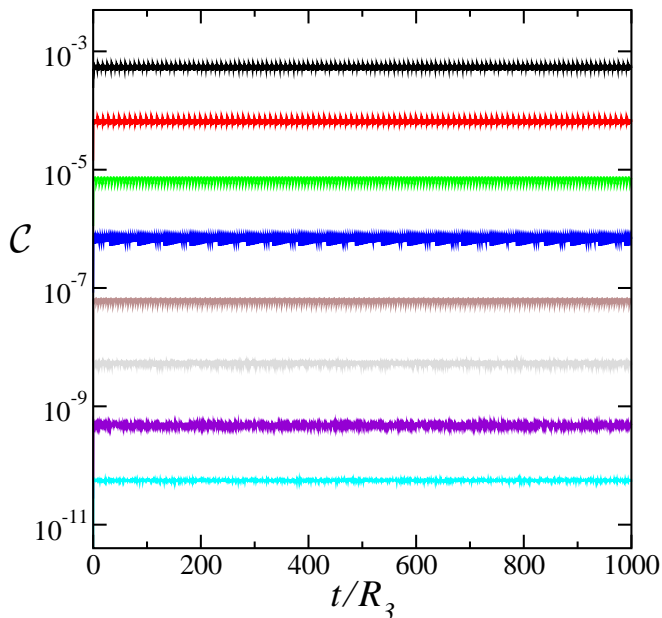


FIG. 11: Constraint norm \mathcal{C} for evolutions (including mode-damping forces) of initial data for the perturbed Einstein-Klein-Gordon solution. Numerical resolutions are the same as those shown in Figs. 1–3.

all of the modes of the Einstein-Klein-Gordon static universe in Sec. VI. We use these analytical expressions to construct initial data for a complicated, time-dependent spacetime having considerable spatial structure. Our numerical evolutions of these initial data converge toward the (small-amplitude) analytical perturbation solution, while the constraints and mode-damping forces converge toward zero, as the spatial resolution is increased.

The numerical tests presented in this paper are all performed on the manifold $R \times S^3$. Nevertheless, we believe that these tests confirm that the multicube methods described in Secs. II and III for solving Einstein’s equation on manifolds with arbitrary spatial topologies have been implemented correctly. In the multicube method, the equations are solved locally within each cubic region \mathcal{B}_A with boundary conditions, cf. Sec. IID, that guarantee that the solution within each region corresponds to the desired global solution. These boundary conditions depend on the topology of the manifold only through their dependence on the reference metric $\tilde{\psi}_{ab}$ and the interface boundary maps $\Psi_{B\beta}^{A\alpha}$. So while the simulations presented here do not test reference metrics or interface boundary maps for a wide range of manifolds with “arbitrary” topologies, they do verify that the basic structure of the boundary conditions that would apply for arbitrary topologies has been done correctly.

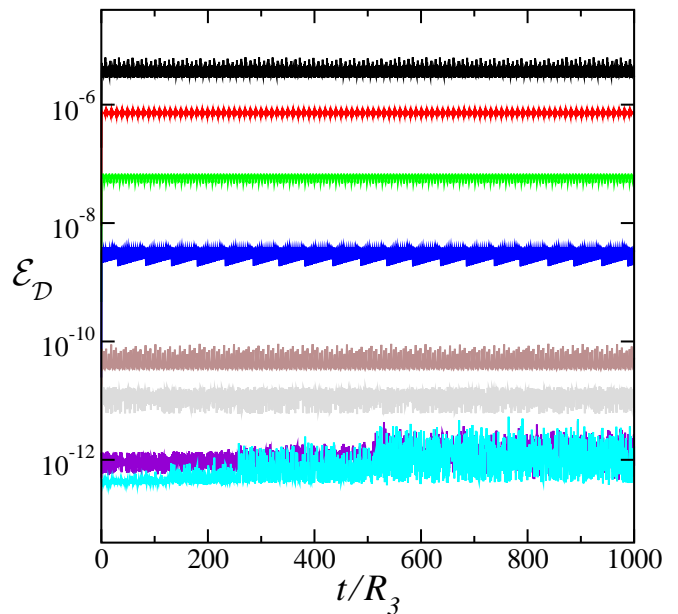


FIG. 12: Norm of the mode-damping forces, \mathcal{E}_D , for evolutions (including mode-damping forces) of initial data for the perturbed Einstein-Klein-Gordon solution. Numerical resolutions are the same as those shown in Figs. 1–3.

Acknowledgments

We thank Michael Holst, James Isenberg, Oliver Rinne, and Manuel Tiglio for helpful discussions concerning this work. We thank the KITP at the University of California at Santa Barbara and the Mathematical Sciences Center at Tsinghua University in Beijing, China, for their hospitality during the time that a portion of this work was performed. We also thank the Center for Computational Mathematics at the University of California at San Diego for providing access to their computer cluster on which the numerical tests reported in this paper were performed. This research has been supported by a grant from the Sherman Fairchild Foundation and by NSF Grants No. PHY1005655 and No. DMS1065438.

Appendix A: Covariant Einstein Constraints

This appendix presents explicit expressions for the covariant constraints of the Einstein evolution system derived in Sec. III in terms of the covariant first-order dynamical fields ψ_{ab} , Π_{ab} , and Φ_{iab} and their spatial derivatives. The primary constraint \mathcal{C}_a of this system, defined in Eq. (19), has the following expression in terms of the first-order fields:

$$\mathcal{C}_a = H_a + g^{ij}\Phi_{ija} + t^b\Pi_{ba} - \frac{1}{2}g_a^i\psi^{bc}\Phi_{ibc} - \frac{1}{2}t_a\psi^{bc}\Pi_{bc}. \quad (\text{A1})$$

The three-index constraint \mathcal{C}_{iab} , defined in Eq. (27), has the following expression:

$$\mathcal{C}_{iab} = \tilde{\nabla}_i \psi_{ab} - \Phi_{iab}. \quad (\text{A2})$$

The spatially covariant analog of the Hamiltonian and momentum constraints of more standard 3+1 representations of Einstein's equation, \mathcal{F}_a , defined in Eq. (38), has the following explicit representation in terms of the first-order fields:

$$\begin{aligned} \mathcal{F}_a \equiv & \frac{1}{2} g_a^i \psi^{bc} \tilde{\nabla}_i \Pi_{bc} - g^{ij} \tilde{\nabla}_i \Pi_{ja} - g^{ij} t^b \tilde{\nabla}_i \Phi_{jba} \\ & + \frac{1}{2} t_a \psi^{bc} g^{ij} \tilde{\nabla}_i \Phi_{jbc} + t_a g^{ij} \tilde{\nabla}_i H_j - g_a^i t^b \tilde{\nabla}_i H_b \\ & + g_a^i \Phi_{ijb} g^{jk} \Phi_{kcd} \psi^{bd} t^c - \frac{1}{2} g_a^i \Phi_{ijb} g^{jk} \Phi_{kcd} \psi^{cd} t^b \\ & + g^{ij} \Phi_{icd} \Phi_{jba} \psi^{bc} t^d - \frac{1}{2} t_a g^{ij} g^{mn} \Phi_{imc} \Phi_{njd} \psi^{cd} \\ & - \frac{1}{4} t_a g^{ij} \Phi_{icd} \Phi_{jbe} \psi^{cb} \psi^{de} + \frac{1}{4} t_a \Pi_{cd} \Pi_{be} \psi^{cb} \psi^{de} \\ & + \frac{1}{2} t_a \Pi_{cd} \Pi_{be} \psi^{ce} t^d t^b + g_a^i \Phi_{icd} \Pi_{be} t^c t^b \psi^{de} \\ & - t^b g^{ij} \Pi_{bi} \Pi_{ja} - \frac{1}{4} g_a^i \Phi_{icd} t^c t^d \Pi_{be} \psi^{be} + 2\Lambda t_a \\ & - g^{ij} \Phi_{iba} t^b \Pi_{je} t^e - \frac{1}{2} g^{ij} \Phi_{icd} t^c t^d \Pi_{ja} - 16\pi T_{ab} t^b \\ & + \gamma_2 (g^{ic} \mathcal{C}_{ida} - \frac{1}{2} g_a^i \psi^{cd} \mathcal{C}_{icd}) - \Delta^b_{ac} t^c \mathcal{C}_b \\ & + 2g^{ij} t^c \psi_{k(j} \tilde{R}^k_{a)ic} - 2\psi^{ij} t^b \tilde{R}^k_{ij(a} \psi_{b)k} \\ & - g_a^i \psi^{bd} t^c \psi_{j(b} \tilde{R}^j_{d)ic} + t_a \psi^{bd} \psi^{ij} \tilde{R}^k_{ij(b} \psi_{d)k}. \quad (\text{A3}) \end{aligned}$$

Similarly, the two-index constraint, \mathcal{C}_{ia} , defined in Eq. (39), is given by the expression

$$\begin{aligned} \mathcal{C}_{ia} \equiv & g^{jk} \tilde{\nabla}_i \Phi_{jka} - \frac{1}{2} g_a^j \psi^{cd} \tilde{\nabla}_i \Phi_{jcd} + t^b \tilde{\nabla}_i \Pi_{ba} \\ & - \frac{1}{2} t_a \psi^{cd} \tilde{\nabla}_i \Pi_{cd} + \tilde{\nabla}_i H_a + \frac{1}{2} g_a^j \Phi_{jcd} \Phi_{ief} \psi^{ce} \psi^{df} \\ & + \frac{1}{2} g^{jk} \Phi_{jcd} \Phi_{ike} \psi^{cd} t^e t_a - g^{jk} g^{mn} \Phi_{jma} \Phi_{ikn} \\ & + \frac{1}{2} \Phi_{icd} \Pi_{be} t_a (\psi^{cb} \psi^{de} + \frac{1}{2} \psi^{be} t^c t^d) \\ & - \Phi_{icd} \Pi_{ba} t^c (\psi^{bd} + \frac{1}{2} t^b t^d) \\ & + \frac{1}{2} \gamma_2 (t_a \psi^{cd} - 2\delta_a^c t^d) \mathcal{C}_{icd} - \Delta^b_{ia} \mathcal{C}_b. \quad (\text{A4}) \end{aligned}$$

Finally, the four-index constraint, \mathcal{C}_{ijab} , defined in Eq. (40), is given by

$$\mathcal{C}_{ijab} = 2\tilde{\nabla}_{[j} \Phi_{i]ab} + \tilde{R}^c_{aji} \psi_{cb} + \tilde{R}^c_{bji} \psi_{ac}. \quad (\text{A5})$$

These expressions for the constraints make it possible to evaluate them easily in terms of the first-order dynamical fields of the system and their spatial derivatives at any instant of time. These expressions are analogous to those for the standard noncovariant generalized harmonic evolution system [2], but the covariant expressions used here depend in critical ways on the geometry of the reference metric $\tilde{\psi}_{ab}$ used to define the covariant derivative $\tilde{\nabla}_i$.

Appendix B: Tensor Harmonics on S^3

This appendix summarizes the basic properties of the three-sphere scalar, vector, and tensor harmonics. These harmonics are defined here as eigenfunctions of the covariant Laplace operator on the three-sphere, based on

the approach developed by Sandberg [21]. The notation introduced here is intended to be simpler and more systematic than that used by Sandberg. Our expressions for the vector and tensor harmonics are also covariant. Covariance allows us to evaluate these tensors using any convenient choice of coordinate basis on S^3 , like the multicube Cartesian coordinates. The angular functions χ , θ , and φ that appear in our expressions are considered to be functions of whatever choice of spatial coordinates is used. Explicit expressions for these angular functions in terms of the multicube Cartesian coordinates are given, for example, in Appendix A.3 of Ref. [1].

The scalar harmonics on the three-sphere are denoted here as $Y^{k\ell m}$, where $k \geq \ell \geq 0$ and $\ell \geq m \geq -\ell$ are integers. These harmonics are defined to be eigenfunctions of the covariant Laplace operator for the standard round metric on S^3 :

$$\nabla^i \nabla_i Y^{k\ell m} = -\frac{k(k+2)}{R_3^2} Y^{k\ell m}, \quad (\text{B1})$$

where ∇_i is the covariant derivative, and R_3 is the radius of the round-sphere metric on S^3 .

The vector harmonics on S^3 can be derived directly from the scalar harmonics. In particular, the three vector harmonics $Y^{k\ell m}_{(0)i}$, $Y^{k\ell m}_{(1)i}$, and $Y^{k\ell m}_{(2)i}$ are given by

$$Y^{k\ell m}_{(0)i} = \nabla_i Y^{k\ell m}, \quad (\text{B2})$$

$$Y^{k\ell m}_{(1)i} = \epsilon_i^{jk} \nabla_j Y^{k\ell m} \nabla_k \cos \chi, \quad (\text{B3})$$

$$Y^{k\ell m}_{(2)i} = \epsilon_i^{jk} \nabla_j Y^{k\ell m}_{(1)k}, \quad (\text{B4})$$

where ϵ_{ijk} is the totally antisymmetric tensor volume element, which satisfies $\nabla_n \epsilon_{ijk} = 0$. These vector harmonics satisfy the following divergence conditions:

$$\nabla^i Y^{k\ell m}_{(0)i} = -\frac{k(k+2)}{R_3^2} Y^{k\ell m}, \quad (\text{B5})$$

$$\nabla^i Y^{k\ell m}_{(1)i} = 0, \quad (\text{B6})$$

$$\nabla^i Y^{k\ell m}_{(2)i} = 0, \quad (\text{B7})$$

and the following eigenvalue equations:

$$\nabla^j \nabla_j Y^{k\ell m}_{(0)i} = \frac{2-k(k+2)}{R_3^2} Y^{k\ell m}_{(0)i}, \quad (\text{B8})$$

$$\nabla^j \nabla_j Y^{k\ell m}_{(1)i} = \frac{1-k(k+2)}{R_3^2} Y^{k\ell m}_{(1)i}, \quad (\text{B9})$$

$$\nabla^j \nabla_j Y^{k\ell m}_{(2)i} = \frac{1-k(k+2)}{R_3^2} Y^{k\ell m}_{(2)i}. \quad (\text{B10})$$

There are six (symmetric) tensor harmonics on S^3 , $Y^{k\ell m}_{(0)ij}$, $Y^{k\ell m}_{(1)ij}$, $Y^{k\ell m}_{(2)ij}$, $Y^{k\ell m}_{(3)ij}$, $Y^{k\ell m}_{(4)ij}$, and $Y^{k\ell m}_{(5)ij}$, which can

be defined in terms of the scalar and vector harmonics:

$$Y_{(0)ij}^{klm} = Y^{klm} g_{ij}, \quad (\text{B11})$$

$$Y_{(1)ij}^{klm} = \frac{1}{2} \left(\nabla_i Y_{(1)j}^{klm} + \nabla_j Y_{(1)i}^{klm} \right), \quad (\text{B12})$$

$$Y_{(2)ij}^{klm} = \frac{1}{2} \left(\nabla_i Y_{(2)j}^{klm} + \nabla_j Y_{(2)i}^{klm} \right), \quad (\text{B13})$$

$$Y_{(3)ij}^{klm} = \nabla_i Y_{(0)j}^{klm} + \frac{k(k+2)}{3R_3^2} Y_{(0)ij}^{klm}, \quad (\text{B14})$$

$$Y_{(4)ij}^{klm} = E^{kl} Y_{(1)ij}^{klm} - \frac{1}{4 \sin^2 \chi} \left(Y_{(1)i}^{klm} \nabla_j \cos \chi + Y_{(1)j}^{klm} \nabla_i \cos \chi \right) \times \{ [\ell(\ell+1) - 2] (E^{kl})^2 + 6 \cos \chi E^{kl} - 4 \}, \quad (\text{B15})$$

$$Y_{(5)ij}^{klm} = \frac{1}{2} \left(\epsilon_i^{sn} \nabla_s Y_{(4)nj}^{klm} + \epsilon_j^{sn} \nabla_s Y_{(4)ni}^{klm} \right). \quad (\text{B16})$$

In Eq. (B15), the quantity $H^{kl}(\chi)$ is the function that transforms S^2 harmonics into S^3 harmonics: $Y^{klm}(\chi, \theta, \varphi) = H^{kl}(\chi) Y^{\ell m}(\theta, \varphi)$, while $E^{kl}(\chi)$ is defined by

$$E^{kl} = \frac{2}{[2 - \ell(\ell+1)] \sin \chi H^{kl}} \frac{d}{d\chi} (\sin^2 \chi H^{kl}). \quad (\text{B17})$$

These tensor harmonics are trace free, $0 = g^{ij} Y_{(1)ij}^{klm} = g^{ij} Y_{(2)ij}^{klm} = g^{ij} Y_{(3)ij}^{klm} = g^{ij} Y_{(4)ij}^{klm} = g^{ij} Y_{(5)ij}^{klm}$, except for $g^{ij} Y_{(0)ij}^{klm} = 3Y^{klm}$. These tensor harmonics satisfy the following divergence conditions:

$$\nabla^i Y_{(0)ij}^{klm} = Y_{(0)j}^{klm}, \quad (\text{B18})$$

$$\nabla^i Y_{(1)ij}^{klm} = \frac{3 - k(k+2)}{2R_3^2} Y_{(1)j}^{klm}, \quad (\text{B19})$$

$$\nabla^i Y_{(2)ij}^{klm} = \frac{3 - k(k+2)}{2R_3^2} Y_{(2)j}^{klm}, \quad (\text{B20})$$

$$\nabla^i Y_{(3)ij}^{klm} = \frac{2[3 - k(k+2)]}{3R_3^2} Y_{(0)j}^{klm}, \quad (\text{B21})$$

$$\nabla^i Y_{(4)ij}^{klm} = 0, \quad (\text{B22})$$

$$\nabla^i Y_{(5)ij}^{klm} = 0, \quad (\text{B23})$$

and the following eigenvalue equations:

$$\nabla^n \nabla_n Y_{(0)ij}^{klm} = -\frac{k(k+2)}{R_3^2} Y_{(0)ij}^{klm}, \quad (\text{B24})$$

$$\nabla^n \nabla_n Y_{(1)ij}^{klm} = \frac{5 - k(k+2)}{R_3^2} Y_{(1)ij}^{klm}, \quad (\text{B25})$$

$$\nabla^n \nabla_n Y_{(2)ij}^{klm} = \frac{5 - k(k+2)}{R_3^2} Y_{(2)ij}^{klm}, \quad (\text{B26})$$

$$\nabla^n \nabla_n Y_{(3)ij}^{klm} = \frac{6 - k(k+2)}{R_3^2} Y_{(3)ij}^{klm}, \quad (\text{B27})$$

$$\nabla^n \nabla_n Y_{(4)ij}^{klm} = \frac{2 - k(k+2)}{R_3^2} Y_{(4)ij}^{klm}, \quad (\text{B28})$$

$$\nabla^n \nabla_n Y_{(5)ij}^{klm} = \frac{2 - k(k+2)}{R_3^2} Y_{(5)ij}^{klm}. \quad (\text{B29})$$

These expressions for the tensor harmonics are equivalent to those given by Sandberg [21].

The scalar and tensor harmonics on S^3 can be computed numerically in a straightforward way. The scalar harmonics Y^{klm} are related to the standard S^2 harmonics $Y^{\ell m}$ by the expression $Y^{klm} = H^{kl}(\chi) Y^{\ell m}(\theta, \varphi)$. The functions $H^{kl}(\chi)$ can be determined numerically for $k = \ell$ and $k = \ell + 1$ by the expressions

$$H^{\ell\ell}(\chi) = (-1)^{\ell+1} 2^\ell \ell! \sqrt{\frac{2(\ell+1)}{\pi(2\ell+1)!}} \sin^\ell \chi, \quad (\text{B30})$$

$$H^{\ell+1\ell}(\chi) = \sqrt{2(\ell+2)} \cos \chi H^{\ell\ell}(\chi), \quad (\text{B31})$$

and for $k > \ell + 1$ using the recursion relation

$$H^{k+2\ell} = 2 \cos \chi \sqrt{\frac{(k+3)(k+2)}{(k+3+\ell)(k+2-\ell)}} H^{k+1\ell} - \sqrt{\frac{(k+3)(k+2+\ell)(k+1-\ell)}{(k+1)(k+3+\ell)(k+2-\ell)}} H^{k\ell}. \quad (\text{B32})$$

This recursion relation for $H^{kl}(\chi)$ is obtained from the standard recursion relation used to determine the associated Legendre functions [22] and the fact that $H^{kl}(\chi)$ is proportional to $Q_{k+1/2}^{\ell+1/2}(\chi)/\sqrt{\sin \chi}$, where $Q_{k+1/2}^{\ell+1/2}(\chi)$ is the associated Legendre function of the second kind [1].

The quantities $E^{kl}(\chi)$, defined in Eq. (B17), can be obtained from $H^{kl}(\chi)$ using the standard expressions for the derivatives of the associated Legendre functions. For $k = \ell$, we have

$$E^{\ell\ell} = -\frac{2 \cos \chi}{\ell - 1}, \quad (\text{B33})$$

while for $k > \ell$, these are given by the recursion relation

$$E^{k\ell} = \frac{2(k+2) \cos \chi}{2 - \ell(\ell+1)} - \frac{2\sqrt{(k+1)(k-\ell)(k+\ell+1)} H^{k-1\ell}}{[2 - \ell(\ell+1)] \sqrt{k}} \frac{H^{k\ell}}{H^{k\ell}}. \quad (\text{B34})$$

-
- [1] L. Lindblom and B. Szilágyi, *J. Comp. Phys.* **243**, 151 (2013).
- [2] L. Lindblom, M. A. Scheel, L. E. Kidder, R. Owen, and O. Rinne, *Class. Quantum Grav.* **23**, S447 (2006).
- [3] A. S. Eddington, *Mon. Not. Roy. Astr. Soc.* **90**, 668 (1930).
- [4] E. Bentivegna and M. Korzynski, *Class. Quantum Grav.* **29**, 165007 (2012).
- [5] E. Bentivegna (2013), arXiv:1305.5576.
- [6] E. Bentivegna and M. Korzynski, *Class. Quantum Grav.* **30**, 235008 (2013).
- [7] L. E. Kidder, L. Lindblom, M. A. Scheel, L. T. Buchman, and H. P. Pfeiffer, *Phys. Rev. D* **71**, 064020 (2005).
- [8] F. Pretorius, *Class. Quantum Grav.* **22**, 425 (2005).
- [9] F. Pretorius, *Phys. Rev. Lett.* **95**, 121101 (2005).
- [10] C. Gundlach, J. M. Martin-Garcia, G. Calabrese, and I. Hinder, *Class. Quantum Grav.* **22**, 3767 (2005).
- [11] M. Ruiz, O. Rinne, and O. Sarbach, *Class. Quantum Grav.* **24**, 6349 (2007).
- [12] J. D. Brown, *Phys. Rev. D* **84**, 084014 (2011).
- [13] T. P. Liu, *J. Diff. Equations* **33**, 92 (1979).
- [14] L. E. Kidder, M. A. Scheel, S. A. Teukolsky, E. D. Carlson, and G. B. Cook, *Phys. Rev. D* **62**, 084032 (2000).
- [15] M. A. Scheel, H. P. Pfeiffer, L. Lindblom, L. E. Kidder, O. Rinne, and S. A. Teukolsky, *Phys. Rev. D* **74**, 104006 (2006).
- [16] M. Scheel, M. Boyle, T. Chu, L. Kidder, K. Matthews and H. Pfeiffer, *Phys. Rev. D* **79**, 024003 (2009).
- [17] B. Szilágyi, L. Lindblom, and M. A. Scheel, *Phys. Rev. D* **80**, 124010 (2009).
- [18] R. C. Tolman, *Proc. Natl. Acad. Sci. (USA)* **20**, 169 (1934).
- [19] J. P. Boyd, *Chebyshev and Fourier Spectral Methods* (Dover Publications, 1999), 2nd ed.
- [20] L. Lindblom and B. Szilágyi, *Phys. Rev. D* **80**, 084019 (2009).
- [21] V. D. Sandberg, *J. Math. Phys.* **19**, 2441 (1978).
- [22] W. H. Press, S. A. Teukolsky, W. T. Vetterling, and B. P. Flannery, *Numerical Recipes in FORTRAN* (Cambridge University Press, Cambridge, England, 1992), 2nd ed.